Ionizing Model to Predict the Clustered in Nucleotide Damage after Low & High LET Radiation

A dissertation submitted to

the Graduate School of the University of Cincinnati

in partial fulfilment of the requirements for the Degree of

Doctor of Philosophy

in the Department of Physics of the College of Arts and Sciences

by

Yusra Zabarmawi

B.S., Medical Physics, Umm Al-Qura University, 2008

M.S., Physics, Pittsburg State University, 2014

Committee Chair: Kay Kinoshita, Ph.D

Abstract

Fast charged particles transfer energy to DNA molecules along their path. The electrons of the DNA along the path are ejected through energy transfer, and this process is called ionization. The linear energy transfer (LET) or density of the ionization differs by the type of radiation. For example, high LET, such as protons, produce the ionization in a dense track compared to low LET radiation, such as electrons or photons. Due to the difference in the LET, damage to the DNA are different even if the absorbed dose is the same. In this study, we construct a statistical model called the Track Model for understanding ionization patterns from charged particle radiation in the DNA. The track model is able to predict the rate of ionization clusters per unit radiation dose, which is likely to be related to DNA base lesions. The cluster is defined as two or more ionizations (holes) within a distance which we call the cluster scale (r_0), which is chosen for the study of base lesions to be the size of the nucleotides $0.34\mathrm{nm}$. We then test various r_0 values to see how the model depends on the cluster scale. We examined published data to interpret the results in terms of the track model result. The rate of DNA base modification induced by high LET radiation is lower than the low LET radiation, which is consistent with the track model, where they originate from a single ionization and not from clustered ionization. We fit data to a curve based on single ionization. The best fit for r_0 is 1 nm.

To my beloved parents

Mohammad Zabarmawi

&

Fatmh Farghl

Acknowledgments

Undertaking this PhD posed abundant challenges, which changed me and my perceptions towards life. It was the enormous support of people around me that helped me to overcome such massive challenges.

First and foremost, I would like to express my sincere gratitude to my advisor Prof. Kay Kinoshita for the continuous support she provided me during my study and associated research. Her endless patience, motivation and vast knowledge helped me throughout the whole process. Her advice aided me through my research and through the writing of the thesis. Without her guidance and dedicated efforts, my PhD study would have never been completed successfully. It was perhaps not possible for me to have any better mentor, motivator, and guide than Prof. Kay Kinoshita.

In addition to my advisor, I would like to thank Prof. Wijewardhana for his tremendous help during the preparatory stage before the qualifier exam. Without his help, I could have never fulfilled my desired objective.

I would also like to sincerely thank Prof. Merino for providing me an opportunity to join his team as an intern and use the laboratory and other research facilities. I would like to convey my heartiest thanks to Prof. Lamba for his insightful comments and inspirations.

I would like to express my indebtedness to Prof. Kogan and Prof. Serota as well for being an inherent part of my thesis committee.

I would like to thank Dr. Safnas AbdulSalam, Gurdat Premnauth, and Prof. Lisa Prevette for helping me in the Chemistry lab.

Lastly but not the least in significance, I would like to thank my family, my parents Mohammad

Zabarmawi and Fatmh Farghl, and my sisters Amani, Manal, and Muna, for supporting me spiritually while I prepared my PhD . I am grateful to my parents for their limitless sacrifice and prayers that sustained me thus far. My friends filled my life with enjoyments and also enlightened me. I would like to thank them all for their support and friendship.

I am immensely grateful to SACM (Saudi Arabian Cultural Mission) for the funding they provided for my PhD Similarly, I am also vastly grateful for the funding I received through UC's LEAF (Leadership, Empowerment, and Advancement of Women Faculty) program for conducting my research activities.

Contents

List of Tables

List of Figures

Chapter 1

Motivation

Ionizing radiation can change the chemical structure of matter. When interacting with a biological system, ionizing radiation can cause cell reproductive death via basic molecular damage in the cell. DNA molecules are considered the most critical target for radiation because they have a large molecular weight and play a central role in cell function[3]. Double strand break (DSB) is considered the most critical type of DNA damage may result in a genetic mutation or death of the cell[5].

Most radiologists have concluded that the quantitative DNA damage after exposure to radiation depends not only on the absorbed dose but also on the radiation quality[6]. High linear energy transfer (LET) radiation, such as protons, produces the ionization in a dense track that leads to high relative biological effectiveness (RBE) compared to low LET radiation, such as photons. However, no universal relationship currently exists between the RBE and the LET. Importantly, explaining the difference between the biological damage of low and high LET requires describing the microscopic spatial distribution of energy deposition in cells.

In this work, we aim to find a general relationship between radiation types and the biological effects of radiation. Our project is based on applying the stopping power theory to DNA, to attain deeper knowledge on the biologically relevant physical effects of different types of radiation. We used a robust experimental method (high performance liquid chromatography (HPLC) in tandem with

mass spectrum (MS)) to detect and analyze the DNA base damage produced by both high and low LET radiation.

We were able to build a track model that shows the relationship between the LET and the rate of clustered ionization in DNA. By comparing the model with the experimental result, we aim to understand the level of the biological effects caused by different types of ionizing radiation.

Chapter 2

Biological Effects of Radiation

2.1 Introduction

Exposing human tissues to ionizing radiation causes a variety of reactions in the cell. Some of these responses lead to cellular death. Many studies indicate that DNA is the principal target of the biological effects of radiation.

2.2 The structure and dimension of DNA

The human DNA molecule is a nucleic acid made of two strands coiled around each other to form a double helix. Each strand has a backbone made of alternating phosphate and sugar groups. Each sugar attaches to one of four bases (Adenine [A], Guanine [G], Cytosine [C], and Thymine [T]). In addition, the two strands are held together by a hydrogen bonding that occurs between pairs of bases at intervals of 0.34 nm along the chain, with a diameter of 2 nm[2]. Adenine always pairs with Thymine, and Cytosine pairs with Guanine. DNA strands store biological information, and each strand has the same biological information.

2.3 Radiation-Induced Damage to DNA

Radiation-induced DNA lesions have been investigated for two types of causes, referred to as the direct effect and the indirect effect.

2.3.1 Direct effect

When any form of radiation is absorbed in biological material, it may interact directly with DNA molecules in the cell. The atoms of a DNA molecule maybe ionized or excited, thus initiating a chain of events that leads to biologic change. This is called a “direct hit “on the DNA by radiation. The direct action is the dominant process for radiation with high linear energy transfer (LET), such as protons[5].

2.3.2 The indirect effect

In an indirect action, ionizing radiation interacts with water molecules surrounding the DNA to produce free radicals. Free radicals, which are molecules containing an unpaired orbital electron in the outer shell, must travel to reach and damage the DNA. This project focused on direct DNA damage. The DNA were irradiated to a dry form to avoid indirect damage.

2.4 Type of DNA damage produced by radiation

Interacting ionizing radiation with DNA causes different types of DNA lesions such as DNA strand breaks and base damage.

2.4.1 Base damage

Base damage is one of the most commonly studied forms of radiation induced damage to DNA. DNA base damage occurs when one or more bases (C, G, A, and T) is damaged or chemically modified by radiation. This type of damage is easy to repair since the cell just replaces the damaged base with the new base[2].

2.4.2 DNA single strand breaks

A single strand break (SSB) is another commonly studied type of radiation-induced DNA damage. SSBs happen when one of the DNA double helices is broken. Single strand breaks are easily repaired using the opposite strand as a template.

2.4.3 DNA double strand breaks

If both strands of the DNA are broken and the breaks are well separated, repair again occurs readily, since the two breaks are handled separately. By contrast, if the breaks in the two strands are opposite one another or separated by only a few base pairs, this may lead to a double strand break. A double strand break is believed to be the most important lesion produced in chromosomes by radiation and this can lead to cell killing[5]. This is because double strand breaks can lead to chromosome aberrations that present problems when the cell attempts to divide.

2.4.4 Clustered lesions

Clustered lesions have two or more different types of damage in near proximity. Even though it is proven that isolated damages can be efficiently repaired, clustered DNA lesions are perceived to be more difficult to repair and may result in genetic mutation[10].

2.5 Techniques to measure DNA damage

2.5.1 Gel electrophoresis

Gel electrophoreses is a method used for separating DNA fragments by size and shape. DNA has a net negative charge that is moved by an electric field through a matrix of agarose gel. The electrophoretic mobility is affected by plasmid [1] DNA shape. For example, supercoiled- undamaged-plasmid migrates quickly. On the other hand, when one of the strands breaks (SSBs), the plasmid becomes like an open loop form. The electrophoretic mobility of this type is smaller than that of

[1]Plasmid is a small,circular and double stranded DNA molecule that separated from chromosomal DNA in bacteria

supercoiled molecules. Moreover, for double-strand breaks (DSBs) DNA molecules have a linear form. Linear DNA mobility in electrophoresis gel is between that of a circle and supercoiled (Figure 2.1). By using ethidium bromide (EtBr) dye [2], which fluoresces under UV light, DNA molecules in gels can be visualized [2].

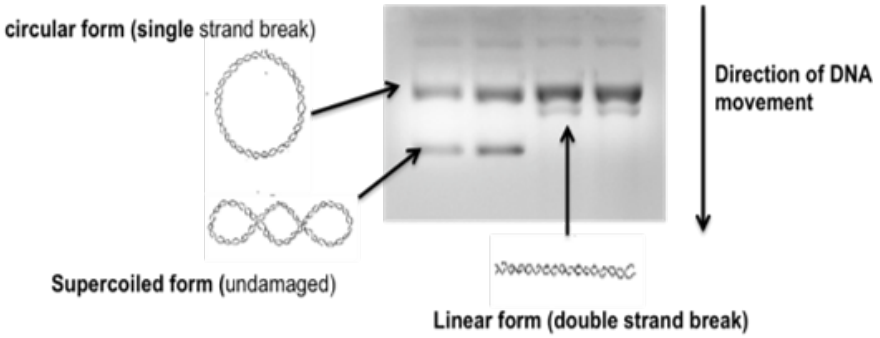

Figure 2.1: Gel electrophoresis. As depicted in the image, DNA travels from the top to the bottom. The top line represents single strand breaks. The second line shows double strand breaks. Lastly, the bottom line represents undamaged DNA

2.5.2 High performance liquid chromatography (HPLC)

The high performance liquid chromatography (HPLC) assay is a powerful tool that can be used for separating and quantifying DNA base lesions[13]. HPLC is a technique to separate, identify, and quantify each component in a sample. The DNA sample is digested into nucleotides. The sample is then pumped at high pressure through a column filled by a solid adsorbent material. Because the nucleotides of modified base all have different flow rates, this leads to the separation of the sample into different components as it moves through the column. Generally, the differential rate is facilitated by the interaction between the sample products and the adsorbent materials[4] . The separated samples are analyzed in a mass spectrometer to identify them. In this project, we use this technique to quantify and identify DNA base lesions.

[2]Ethidium bromide intercalate between DNA molecules and allow detection of DNA fragments in gels. Ethidium bromide is added to agarose gel to visualize of the fragments within the gel.

2.6 Cellular response to radiation

2.6.1 Cell Survival curve

Every cell in the human body has the same DNA. However, various cell types react to radiation differently. These differences can be attributed to divergence in the cellular response. One way of measuring the cellular response to radiation is by finding the cell survival fraction, which is the fraction of cells that is able to divide after radiation exposure. A cell survival curve represents the relationship between the fraction of surviving cells and the radiation dose (Figure 2.2). A survival curve is plotted on a log-linear scale, with dose on the linear scale and survival fraction on the logarithmic scale. The shape of the curve changes with the radiation type. For low LET radiation, the curve is characterized by a curvature— known as a shoulder —over the low dose. For high LET radiation, the curve is more linear .

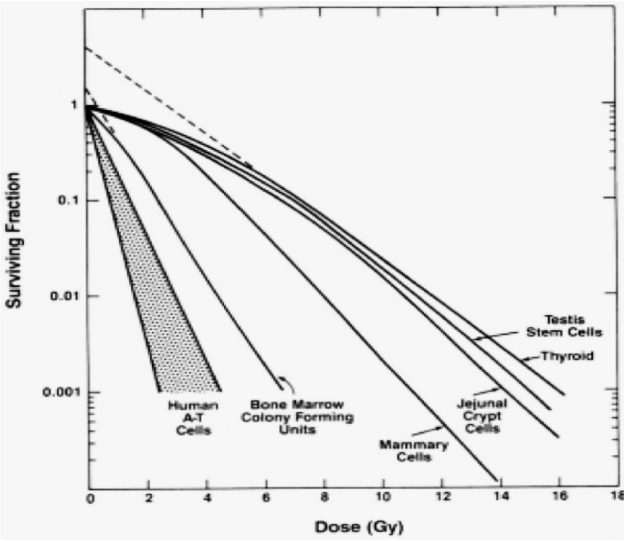

Figure 2.2: Cell survival curves for different human tissue vs dose in X-rays [5].

2.6.2 Linear quadratic model to describe cell survival curve

The Linear-quadratic (LQ) model [5] is used to describe survival curves. LQ theory states that cell inactivation happen under two conditions single-hit lethal event or sublethal event (two hits). The

most common expression is

$$-\ln S = \alpha D + \beta D^2$$

Where S is the fraction of cells,α and β are constants, and D is the dose. The linear term αD represents cell death due to single lethal hit to the DNA and βD^2 the quadratic term is meant to take into account the cell death due to two hits to the DNA. LQ model fits the cell surviving curve fairly well and is useful. However, to date, no one at this point truly knows how to explain the curve from a realistic and advanced mathematical point of view because the underlying mechanism of DNA damage, repair, and cell killing is not understood completely.

Chapter 3

Radiation Interaction with Biological System

3.1 Theory of stopping power

Ionizing radiation transfers energy by ejecting orbital electrons from an atom or molecule. The energy transfer from the charged particle to each electron in the matter is small; therefore, the kinetic energy of the charged particle is only spent after many interactions. Stopping power describes the energy loss of the charged particle as it penetrates into an absorber [8]. Stopping power is determined by different characteristics of the charged particle, including the charge and velocity, together with the characteristics of the absorbing medium, such as the atomic number and density, mean ionization potential.

3.1.1 Calculateion of stopping power

As a particle with charge z, speed v, and energy E traveling a distance x into a material of electron density N and mean ionization potential I, which is described below, the stopping power of the material can be calculated using the Bethe-Bloch formula [1].

$$S = -\frac{dE}{dx} = \frac{4\pi N z^2 e^4}{mv^2}[\ln\frac{2mv^2}{I} - \ln\frac{1}{1-\beta^2} - \beta^2] \tag{3.1}$$

In this formula, e is the magnitude of the electron charge, m is the electron rest mass, c is the speed of light and $\beta = v/c$

3.1.2 Mean ionization / excitation energy

Charged particles interact mainly with bound electrons in the medium, causing excitation or ionization. The energy transfer must exceed the excitation or binding energy of the orbital electron. The more energy is needed to free the electrons, the less likely it is to happen. The stopping power depends on the distribution of electron binding energies of the target material (mean ionization potential) [8],I. The I value in eV for a compound or mixture can be estimated using the Bragg rule [1].

$$N \ln I = \sum_n N_n \ln I_n \tag{3.2}$$

In this formula, I_n is the atomic mean ionization potential per electron for that element, N_n is the number of electrons associated with element n and
$N = \sum_n N_n$

3.1.3 Application of the stopping power theory to the biological system

In this section, we aim to calculate the mean ionization energy of electrons in DNA and the stopping power for minimum ionizing charged particles in DNA.

Effective ionization energy of DNA

DNA strands are composed of four types of nucleotides: C, G, A and T. The number of electrons per DNA nucleotide is C $[C_9H_{14}N_3O_8P] = 168$ electrons, G $[C_{10}H_{14}N_5O_8P] = 188$ electrons ,A $[C_{10}H_{14}N_5O_7P] = 180$ electrons and T $[C_{10}H_{14}N_2O_8P] = 167$ electrons.
The mean ionization energy in eV for H, C, N, O and P is 17.8, 77.3, 99.5, 98.5 and 172 respectively [1]. By using the Bragg rule for each nucleotide, we have determined that the mean ionization energy is $I_C = 83.14$ eV , $I_G = 84.07$ eV, $I_A = 83.48$ eV and $I_T = 82.30$ eV The average of these values is found to be $83.2\ eV$.

The stopping power for minimum ionizing particles in DNA

The stopping power of charged particles is approximately proportional to $\propto 1/v^2$, where v represents the speed of the charged particle. When $v \approx 0.95c$, the stopping power has its minimum value, and particles at and above this speed are called "minimum ionizing." The stopping power or LET (section 3.3.1) (for this study, the stopping power is treated as being equal to LET) of a singly charged minimum ionizing particle, often called "Low- LET" radiation, includes electrons and gamma rays.

The stopping power for minimum ionizing particles in DNA was estimated using the Bethe-Bloch equation

$$S = -\frac{dE}{dx} = \frac{4\pi k_0^2 N z^2 e^4}{mc^2\beta^2}[\ln \frac{2mc^2\beta^2}{I(1-\beta^2)} - \beta^2] \tag{3.3}$$

$$= \frac{4\pi k_0^2 N z^2 e^4}{mc^2\beta^2}[\ln 2mc^2\beta^2 - \ln I(1-\beta^2) - \beta^2]$$

$$= \frac{4\pi k_0^2 N z^2 e^4}{mc^2\beta^2}[\ln \frac{2mc^2\beta^2}{1-\beta^2} - \beta^2 - \ln I_{eff}] \tag{3.4}$$

If the constants are evaluated the equation reduces to

$$-\frac{dE}{dx} = \frac{5.08 \times 10^{-31} z^2 N}{\beta^2}[F(\beta) - \ln I_{eff}] \tag{3.5}$$

where $F(\beta) = \ln \frac{2mc^2\beta^2}{1-\beta^2} - \beta^2 = \ln \frac{1.02 \times 10^6 \beta^2}{1-\beta^2} - \beta^2$

The average molecular weight of the base pair is 6.77×10^2 g/mole and the average number of electrons per base pair is 3.51×10^2 electrons.

The DNA density is estimated to be $1.4\ g/cm^3$ and for density of electrons, N is

$$N = 6.02 \times 10^{23} \times \frac{1.4}{6.77 \times 10^2} \times 3.51 \times 10^2 \tag{3.6}$$

$$= 4.37 \times 10^{23} electrons/cm^3$$

For minimum ionizing particle $\beta = 0.95$.

As we found before, $I_{eff} = 8.32 \times 10^1\ eV$. The stopping power for minimum ionizing particles – we will use the term "low-LET" for these particles for the reminder of this thesis- is

$$-\frac{dE}{dx} = \frac{5.08 \times 10^{-31} \times 4.37 \times 10^{23}}{0.90} = 2.64 MeV/cm \tag{3.7}$$

$$= 0.26 keV/\mu m$$

3.2 Hole density & linear hole density produced by a charged particle along its track

The Dose is defined as the energy deposited in the material per mass. A common unit of measure for dose in the cancer medicine is Gray (Gy) where

$$1\mathrm{Gy} = 10^4 \mathrm{erg/g} = 6.24 \times 10^{15} \mathrm{eV/g} \tag{3.8}$$

The mass of 1 base pair of DNA (M) is 1.08×10^{-21} g. For our convenience the mass is converted to $\mathrm{Mbp} = 1 \times 10^6$ bp unit.

$$1\mathrm{g} = 0.92 \times 10^{15} \mathrm{Mbp}$$

The energy deposited per dose (Gy) per Mbp= $\frac{6.24 \times 10^{15} \mathrm{eV/g}}{0.92 \times 10^{15} \mathrm{Mbp}} = 6.78$ eV/Mbp. The hole density in the DNA target is proportional to the dose D and inversely proportional to the mean ionizing potential. Thus, the hole density,in per Gy per Mbp,is

$$n_1 = \frac{energy/Gy/Mbp}{I_{eff}} = \frac{6.78 eV/Mbp}{8.32 \times 10^1 ev} = 8.14 \times 10^{-2}/Mbp \tag{3.9}$$

The linear hole density λ_{LET} on the path of a particle in DNA is

$$\lambda_{LET} = \frac{LET}{I_{eff}} \tag{3.10}$$

For low-LET radiation, the linear hole density λ_{min} on the path of an I_{min} (minimum ionizing particle) particle in DNA is

$$\lambda_{min} = \frac{0.26keV/\mu m}{83.2eV} = 3.17/\mu m \tag{3.11}$$

3.3 Radiation quality

3.3.1 LET dependence

Biological effect is not only dependent on the absorbed dose but also on the radiation quality. For example, one Gy of alpha radiation causes more biological damage than one Gy of photon radiation because the distribution of the ionization along the track of the photon or charged particle is different. The effectiveness of the given dose increases with the ionization density which is related to the linear energy transfer (LET). LET is the energy transfer to the material per unit distance of the track length. High LET radiation such as heavy ions and protons produce the ionization in a dense track which may produces a complex DNA damage.

The difference due to LET is measured by Relative biological effectiveness (RBE). RBE is a quantitative description of the dependence of the radiation quality on biological effect. RBE is the ratio of the doses of two types of ionizing radiation that give the same biological damage. Higher RBE correlates with greater DNA damage per dose, as measured experimentally. However, to date, this relationship couldn't be explained very well by physical modeling .

In this project, we aim to understand the biological damage by correlating rates of various types of ionization clustering and lethal types of DNA damage.

Chapter 4

Cluster Distribution in DNA Molecules in the Track Model

4.1 Introduction

Interactions of charged particles with DNA may damage the DNA helix. In this project, we construct a statistical model (Track Model) to calculate the clustered ionization rate in DNA nucleotide and then compare rates with experimental measurements of DNA base modification (next chapters).

4.2 The Track Model Theory

The track model is based on the theory of the stopping power, which explains the energy loss of charged particles when interacting with matter. The primary mode of energy exchange with the DNA is through ionization or excitation of electrons in the double helix. For our model, we find the ionization cluster rate in DNA (will focus here on base modifications) caused by different type of radiation. We hypothesize that the "Cluster" - two or more holes within a track length,"r_0",which we call the "clustering scale" - is related to the biological damage.

4.3 Cluster Size distribution "nucleotides level"

4.3.1 The cluster scale r_0

In this project, we focus on studying DNA base modification, so the definition of a cluster in the track model is adjusted to fit the HPLC method, where the damage is detected on nucleotides. We defined the cluster as two or more holes separated by $r_0 = 0.34$nm where r_0 is the approximate size of a nucleotide molecule.

4.3.2 The mean number of holes $\bar{n}_h$ per segment length r_0

If all holes are produced in a DNA unit mass M, delivered by tracks with hole density λ_{LET} in a dose D, the number of holes N is

$$N = n_1 DM$$

from which the total associated track length per mass per unit dose T follow:

$$T = \frac{N}{\lambda_{LET}} = \frac{n_1 DM}{\lambda_{LET}} \tag{4.1}$$

To quantify clusters on the track, we consider that on a random segment of length r_0 will have a mean number of holes $\bar{n}_h$, the mean number of holes $\bar{n}_h$ per segment is

$$\bar{n}_h = \lambda_{LET} \times r_0 \tag{4.2}$$

For low-LET radiation, the mean hole number $\bar{n}_h$ is

$$\bar{n}_h = \lambda_{min} \times r_0 = 3.17 \times 0.34 \times 10^{-3} = 1.07 \times 10^{-3} holes$$

4.3.3 The probability of the cluster

In the track model, we define the cluster as an occurrence of $j \geq 2$ holes occurring within a track segment of length r_0.

For any segment, the cluster probability, P_{cl}, that j holes are found is distributed according to Poisson distribution.

$$P\left(j;\bar{n}_h\right) = \frac{e^{-\bar{n}_h}\bar{n}_h^j}{j!} \tag{4.3}$$

Where $\bar{n}_h$ is the mean number of holes and j "$complexity$" is the number of holes in the segment.

The cluster probability $j \geq 2$ is the probabilities of the clusters for $j = 0$, $j = 1$, subtracted from unity:

$$P\left(\geq 2;\bar{n}_h\right)) = 1 - P\left(0;\bar{n}_h\right) - P\left(1;\bar{n}_h\right) = 1 - e^{-\bar{n}_h}(1+\bar{n}_h)$$

For low-LET radiation, where $\bar{n}_h = 1.07 \times 10^{-3}$, the probabilities for $j = 0$, and $j = 1$ are

$$P\left(0;\bar{n}_h\right)) = e^{-\bar{n}_h} = 0.998$$

$$P\left(1;\bar{n}_h\right)) = e^{-\bar{n}_h}\bar{n}_h = 1.061 \times 10^{-3}$$

The probability that the cluster has $j \geq 1$ is the probability of the cluster at $j = 0$ subtracted from unity

$$P\left(\geq 1;\bar{n}_h\right)) = 1 - P\left(0;\bar{n}_h\right) = 1 - e^{-\bar{n}_h}$$

$$1 - 0.99 = 1.061 \times 10^{-3}$$

The probability that the cluster has $j \geq 2$ is

$$P\left(\geq 2;\bar{n}_h\right)) = 1 - e^{-1.37\times10^{-3}}(1 + 1.37 \times 10^{-3}) = 5.640 \times 10^{-7}$$

The value of $\bar{n}_h$ is proportional to the LET and thus affects the clustering rates. To illustrate

the effect, the corresponding rates for 100 times minimum ionizing, $\lambda = 3.17 \times 10^2/\mu m$, are calculated for 1 Gy dose (Tables 4.1, 4.2). The rate of clustering is low for low-LET radiation and significant at the higher LET.

The mean number of holes and the probability were calculated for $r_0 = 0.2$ nm, 0.34 nm, 0.5 nm, 0.8 nm and 1 nm, respectively (Tables 4.1,4.2) to probe the sensitivity of our prediction to assumptions about r_0.

r_0 nm	$\bar{n}_h$	$P_{cl}(j \geq 1)$	$P_{cl}(j = 1)$	$P_{cl}(j \geq 2)$
0.2	0.62×10^{-3}	6.24×10^{-4}	6.25×10^{-4}	0.19×10^{-6}
0.34	1.06×10^{-3}	1.06×10^{-3}	1.06×10^{-3}	0.56×10^{-6}
0.5	1.56×10^{-3}	1.56×10^{-3}	1.56×10^{-3}	1.21×10^{-6}
0.8	2.50×10^{-3}	2.49×10^{-3}	2.49×10^{-3}	3.11×10^{-6}
1	3.12×10^{-3}	3.12×10^{-3}	3.11×10^{-3}	4.87×10^{-6}

Table 4.1: Illustrate the mean number of holes and the cluster probability for minimum ionizing particle $0.26\ keV/\mu m$

r_0 nm	$\bar{n}_h$	$P_{cl}(j \geq 1)$	$P_{cl}(j = 1)$	$P_{cl}(j \geq 2)$
0.2	6.29×10^{-2}	6.09×10^{-2}	5.90×10^{-2}	0.18×10^{-2}
0.34	1.60×10^{-1}	1.00×10^{-1}	9.55×10^{-2}	0.52×10^{-2}
0.5	1.56×10^{-1}	1.44×10^{-1}	1.33×10^{-1}	1.10×10^{-2}
0.8	2.51×10^{-1}	2.22×10^{-1}	1.95×10^{-1}	2.68×10^{-2}
1	3.14×10^{-1}	2.69×10^{-1}	2.29×10^{-1}	4.04×10^{-2}

Table 4.2: Illustrate the mean number of holes and the cluster probability for$100\times$ minimum ionizing particle $26\ keV/\mu m$

To obtain the mean number of clusters $\bar{N}_{clus}$ with complexity j in a given amount of DNA, we multiply the probabilities by the the number of segments $N_{seg} = T/r_0$

$$\bar{N}_{clus}(j) = N_{seg} P(j; \bar{n}_h) \tag{4.4}$$

For 1 Gy of radiation in 1 Mbp the track length is

$$T = \frac{n_1}{\lambda_{LET}}$$

from which the N_{seg} follow:

$$N_{seg} = \frac{T}{r_0} = \frac{n_1}{\lambda_{LET} \times r_0} = \frac{n_1}{\bar{n}_h} \tag{4.5}$$

from which the mean number of cluster $\bar{N}_{clus}$ per Gy per Mbp is

$$\bar{N}_{clus}(j) = \frac{n_1}{\bar{n}_h} \frac{e^{-\bar{n}_h} \bar{n}_h^j}{j!}$$

$$\bar{N}_{clus}(j) = n_1 e^{-\lambda_{LET} \times r_0} \frac{(\lambda_{LET} \times r_0)^{j-1}}{j!} \tag{4.6}$$

where the the hole density $n_1 = 8.14 \times 10^{-2}/Mbp$, $\lambda_{LET} = LET/I_{eff}$ where I_{eff} is $83.2eV$, and j is the complexity.

The mean numbers of clusters $\bar{N}_{clus}$ per Gy per Mbp for different r_0 values are shown in Tables 4.3 and 4.4.

r_0 nm	N_{seg}	$P_{cl}(j \geq 1)/Gy/Mbp$	$P_{cl}(j = 1)/Gy/Mbp$	$P_{cl}(j \geq 2)/Gy/Mbp$
0.2	1.30×10^2	8.13×10^{-2}	8.13×10^{-2}	2.54×10^{-5}
0.34	0.76×10^2	8.13×10^{-2}	8.13×10^{-2}	4.32×10^{-5}
0.5	0.52×10^2	8.13×10^{-2}	8.12×10^{-2}	6.35×10^{-5}
0.8	0.32×10^2	8.13×10^{-2}	8.11×10^{-2}	1.01×10^{-4}
1	0.26×10^2	8.12×10^{-2}	8.11×10^{-2}	1.26×10^{-4}

Table 4.3: The cluster rate per Gy per Mbp ,$\bar{N}_{clus}$, for minimum ionizing particle, LET= 0.26 $keV/\mu m$, for five values of r_0.

r_0 nm	N_{seg}	$P_{cl}(j \geq 1)/Gy/Mbp$	$P_{cl}(j = 1)/Gy/Mbp$	$P_{cl}(j \geq 2)/Gy/Mbp$
0.2	1.29	7.88×10^{-2}	7.64×10^{-2}	2.45×10^{-3}
0.34	0.76	7.77×10^{-2}	7.31×10^{-2}	4.02×10^{-3}
0.5	0.52	7.53×10^{-2}	6.96×10^{-2}	5.73×10^{-3}
0.8	0.32	7.19×10^{-2}	6.32×10^{-2}	8.67×10^{-3}
1	0.25	6.98×10^{-2}	5.94×10^{-2}	1.04×10^{-2}

Table 4.4: The cluster rate per Gy per Mbp , $\bar{N}_{clus}$, for $100\times$ minimum ionizing particle, LET= 26 $keV/\mu m$, for five values of r_0.

4.4 Track Model Result

Figure 4.1 shows the clustering rate per Gy per Mbp as a function of LET. The values of the LET are displayed in the range 0.2 - 5×10^2 $\mathrm{keV}/\mu\mathrm{m}$. Curve 1 represents the survival curve (0 holes) which is decreased for increasing LET values. Curve 2 displays the rate for single ionization 1 hole, 0 clusters ($j = 1$). Curve 3 and 4 the cluster size is 2 and 3 holes respectively.The cluster rate increase slightly with LET and finally the cluster rate starts to decrease at highest LET value $\approx 5 \times 10^2$ $\mathrm{keV}/\mu\mathrm{m}$. The reason for this decreases would be because at high LET the hole density is high leading to holes being concentrated in fewer clusters. In other words, at high LET each cluster will contain more holes so that there is a few clusters to go around.

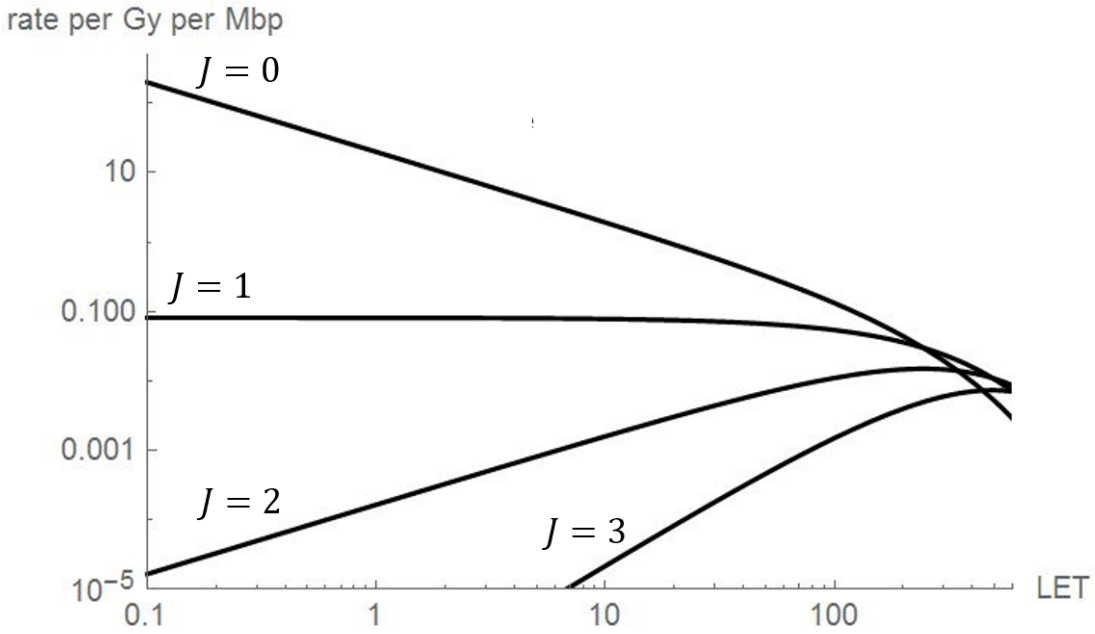

Figure 4.1: The Track Model: the cluster rate per Gy per Mbp (y-axis) vs the LET (x-axis). The first curve from the top ($j = 0$) represents the survival curve. the second curve ($j = 1$) represents the damaged from single ionization. The third and fourth curves ($j = 2$ and $j = 3$) represent the damage from clustered ionization.

4.4.1 Testing different r_0 values in the track model

In this section, the sensitivity of the track model result to r_0 value was tested (Figure 4.2). The

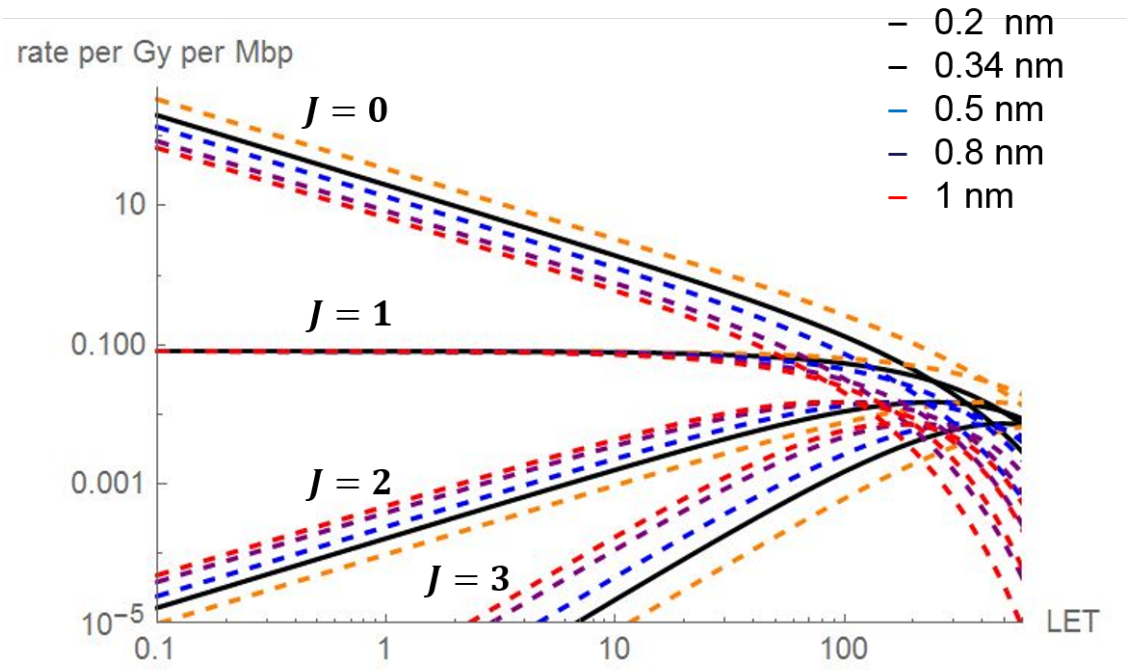

Figure 4.2: Sensitivity of the Track model to r_0 values. r_0 = 0.2nm (dashed orange), $r_0 = 0.34\text{nm}$ (black), $r_0 = 0.5\text{nm}$ (dashed blue), $r_0 = 0.8\text{nm}$ (dashed purple), and $r_0 = 1\text{nm}$ (dashed red). The shape of each curve is insensitive on r_0 values.

ratio between low LET value ($0.26\ keV/\mu m$) to high LET value($25\ keV/\mu m$) in the track model was then calculated (Table 4.5 and Figure 4.3).

By examining the calculated rates for different r_0 values in Tables 4.3 and 4.4, the number of segments per Mbp, N_{seg}, varies over the range of r_0 values by a factor of five. However, for the clustering rate, at $j = 1$ the result is almost constant. At $j \geq 2$ the numbers vary by a factor of five. The rate for producing a particular lesion may be less than the clustering rate, i.e. has an "efficiency" $< 100\%$. However, it is reasonable to assume that an efficiency that is constant for a given cluster index, such as the ratio between high to low LET (Table 4.5), changes a lot less than the rate of ionization clustering. By the same reasoning, we can conclude that the shape of the rate vs LET in the track model has low dependence on r_0.

$r_0\ nm$	$R_{\geq 1}(j \geq 1)$	$R_1(j = 1)$	$R_2(j = 2)$	$R_3(j = 3)$
0.20	1.00	0.91	1.12×10^2	1.46×10^4
0.34	0.90	0.90	1.15×10^2	1.46×10^3
0.50	0.83	0.89	1.09×10^2	1.29×10^4
0.80	0.83	0.75	1.01×10^2	1.21×10^4
1.00	0.74	0.74	9.78×10^1	1.19×10^4

Table 4.5: The ratio between high to low LET radiation in the track model where $R_{\geq 1}$,R_1 ,R_2 and R_3 is the ratio with complexity index $\geq$ 1, 1, 2 and 3 respectively

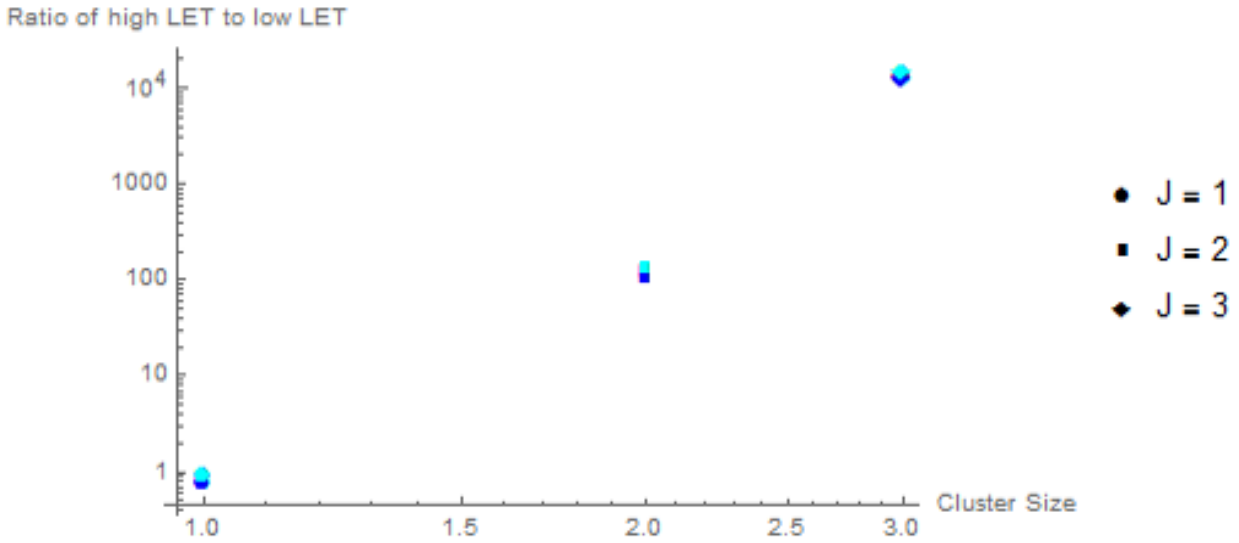

Figure 4.3: The ratio of the clustering rates for $j = 1, 2, 3$ of high LET value($25\ keV/\mu m$) to low LET value ($0.26\ keV/\mu m$) in the track model for different r_0 values (0.2 nm (cyan), 0.34 nm (black), 0.5nm (purple), 0.8nm (green) and 1nm (blue)).

Chapter 5

Analysis of DNA base lesions from UV Radiation Using two analytical Methods (Gel Electrophoresis and HPLC)

5.1 Introduction

Ionizing radiation causes different types of DNA damage such as strand breaks and base damage. There are different methods to quantify and to analyze DNA base modifications, such as gel electrophoresis and high-performance liquid chromatography (HPLC). In this chapter, we learned how to use these techniques and how to analyze the result.

Gel electrophoresis is the technique that is used to separate DNA according to size and shape (as discussed in 2.5.1). DNA base lesions is then detected by treating the DNA samples with the base excision repair enzymes such as Fpg (fomamidopyrimidine - DNA glycosylase), which can recognize the damaged bases from double stranded DNA and remove them by causing additional breaks to the DNA strands, which can be detected through gel electrophoresis.

High performance liquid chromatography (HPLC) tandem mass spectrometer is a sensitive technique used to identify and quantify various types of nucleotides. It is used to separate, identify, and quantify each element in a DNA sample. The process includes pumping a liquid solvent (mobile

phase) with the sample that contain the digested DNA through a column filled with a solid adsorbent material (stationary phase). Due to the different interactions between the adsorbent material and the sample mixture, each component moves at different speeds, causing separation of the components. The mobile phase usually consists of a mixture of solvent (water and acetonitrile). HPLC mixes two solvents (called solvent A and solvent B) together in ratios that change over time, producing a composition gradient in the mobile phase. Many different types of columns (stationary phase) are used in HPLC. These columns are filled with adsorbent material that varies in particle size and surface chemistry. There are different types of detectors used in HPLC. In this experiment, HPLC uses a UV detector and because each molecule of the component has a different absorption coefficient, each can be detected, and quantified.

In this chapter, we designed this training experiment to study DNA base lesions caused by UV radiation using gel electrophoresis and HPLC . We exposed plasmid DNA (pUC19) to UV light (375nm). Direct 375 nm UV on DNA causes no measurable damage. Therefore, we use a cellular photosensitizer, riboflavin, which is excited by absorption of the UV, and interact with the DNA to cause strand breaks [7]. After irradiation, the gel electrophoresis and the HPLC methods were used to quantify and analyze DNA base damage.

5.2 Gel electrophoresis

5.2.1 Identify DNA strand breaks

$5.5\ \mu l$ of the plasmid DNA, pUC19 double stranded plasmid, with final concentration $50\ ng/\mu l$ was mixed with $10\ \mu l$ of $50\ \mu M$ of riboflavin, $27.5\ \mu l$ of $50\ mM$ buffer solution, and $68\ \mu l$ of water. The mixture was then divided into $10\ \mu l$ portions into 10 different 1.5 microcentrifuge tubes. Different samples without riboflavin were also prepared. The sample tubes with the lid open were then irradiated with a LED with $3\ mW$ of radiative flux lamp at $375\ nm$ (Figure 5.1). During photolysis, the samples were held at a distance of $5.5\ cm$ from the UV source for different lengths of time. After irradiation, the samples were mixed with $4\ \mu l$ of agarose gel loading buffer.

Then, the samples were loaded into the slots of the submerged gel. The voltage was then applied ($4\ V/cm$). The gel was imaged on a transilluminator.

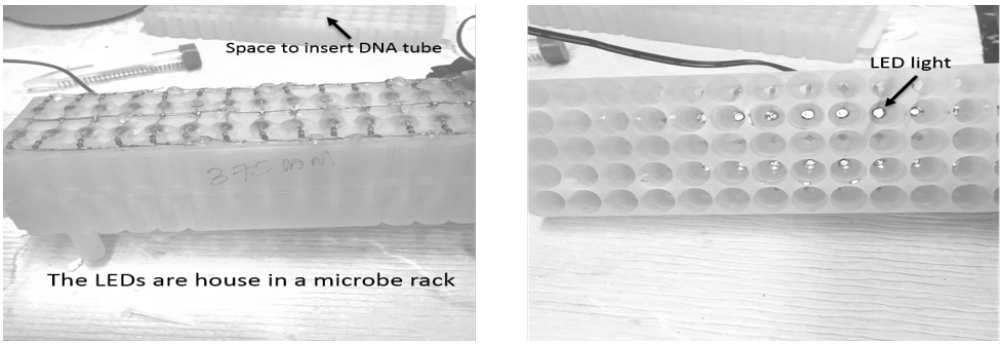

Figure 5.1: Box where the sample irradiate to the UV Light (375 nm). The samples were placed with open lid in 5.5cm from the LED light (3 mW) for different length of time(0 min, 30min ,and 60min).

Result and discussion

The aim of this project is to use gel electrophoresis to quantify DNA strand breaks caused by UV light. To analyze and quantify the DNA damage, the gel analysis software $ImageQuant$, which uses brightness contrast to quantify band intensities.

Figure 5.2 shows the gel electrophoresis result. The lowest band represents undamaged DNA. In contrast, the highest band illustrates damaged DNA via single strand breaks. The first group in Figure 5.2 on the left (DNA+UV) represent the DNA damage with UV light in the absence of riboflavin. The second group, on the right (DNA + UV+ RIB), shows the results in the presence of the UV and riboflavin.

In Figure 5.3, the intensity of the undamaged DNA, survival fractions, vs time (0 min, 30 min and 60 min) was measured. We conclude that the percentage of undamaged DNA with riboflavin decreases exponentially (Figure 5.3b) with exposure time.

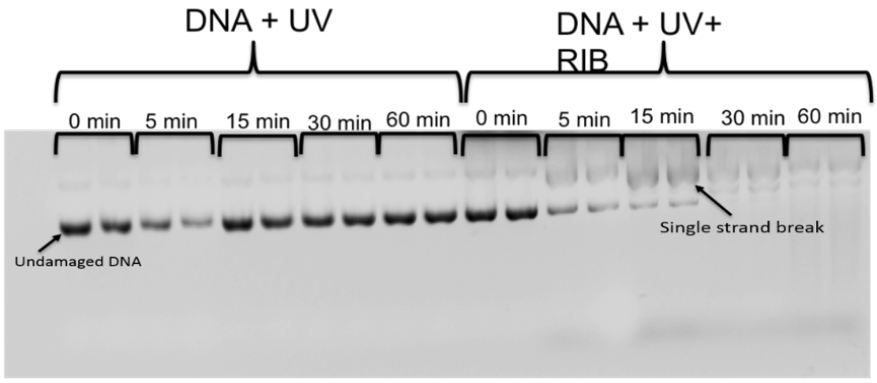

Figure 5.2: Gel electrophoresis result for different conditions of exposure, for (Left) DNA without riboflavin (right) DNA with riboflavin.The lowest band represents undamaged DNA while the highest band represents single strand breaks.

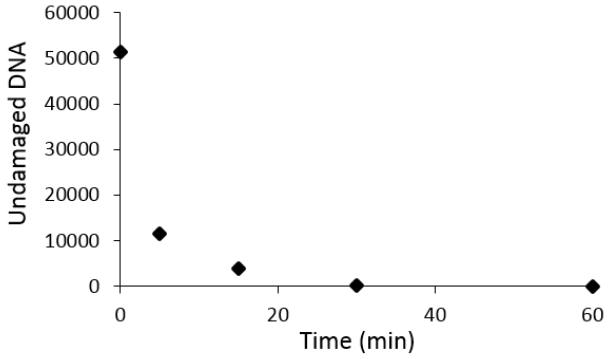

(a)

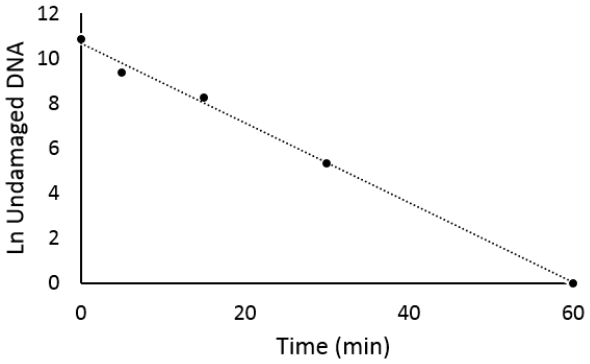

(b)

Figure 5.3: Plots of DNA strand breaks from UV light in the present in the riboflavin for different time period (0 min, 30min and 60 min). b) Log plot of undamaged DNA for different time.These results were obtained by gel electrophoresis

5.2.2 Identify DNA base lesions

In this experiment, $20\ \mu l$ of the plasmid DNA (pUC19) was mixed with $40\ \mu l$ of $50\ \mu M$ of riboflavin, $30\ \mu l$ of $50\ mM$ buffer solution, and $70\ \mu l$ of water. The mixture was then divided into $10\ \mu l$ portions into 16 different 1.5 microcentrifuge tube. The samples were then irradiated in the same way as in section 5.2.1. After irradiation, $0.5\ \mu l$ of $8,000\ U/ml$ of Fpg was added to half of the sample tubes. The samples were then loaded to the gel and visualized.

5.3 Quantifying DNA base lesions by HPLC Method

In this section, the DNA base lesions were quantified by using the HPLC method. To prepare the samples, $50\ \mu l$ of pUC19 with final concentration $50\ ng/\mu l$ was mixed with $100\ \mu l$ of $50\ \mu M$ of riboflavin, $250\ \mu l$ of $50\ mM$ buffer solution, and $609\ \mu l$ of water. The mixture was then divided into $100\ \mu l$ portions into 10 different 1.5 microcentrifuge tube. The samples were then irradiated in the same way as described in section 5.2.1. After irradiation, the samples were made $10\times$ more concentrated via SpeedVac on a high drying rate for 5 hours. The samples were then mixed with $33\ \mu l$ of buffer. The DNA was then digested into single nucleosides (A, C, G, and T and other compounds) by adding $2\ \mu l$ of $1\ U/\mu l$ of Calf Intestinal Alkaline Phosphatase (CIAP), which was purchased from Invitrogen, a subsidiary of Thermo Fisher Scientific. Samples were then incubated for 90 min at 37^0C. Subsequently, $1\ \mu l$ of $0.1\ U/\mu l$ snake venom phosphodiesterase, which was obtained from Worthington Biochemical Corporation Co (Lakewood, NJ), was added, and the samples were incubated for 90 min at 37^0C. Then, $2.5\ \mu l$ of $3\ U/\mu l$ of deoxyribonuclease was added, and the samples were incubated for 90 min at 37^0C. After that, $55\ \mu l$ of water was added to the samples. After digestion, an Agela technologies C18 $[5\mu m, 100A, 4.6 \times 100mm]$ column, a stationary phase, was used for separation of the DNA nucleotides by linear gradient of water [solvent A contain 98% water and 2% acetonitrile, and solvent B contain 95% acetonitrile and 5% water] (mobile phase) over several minutes. The HPLC analysis was performed for 24 min after injection. The absorbance was monitored at 240 nm. The data were quantified using a 32 Karat HPLC software.

5.3.1 HPLC result

In this study we aim to quantify and identify the DNA base lesions that are caused by UV radiation by using the HPLC method. HPLC is able to separate and identify the nucleotides in the sample. To identify each peak from the HPLC chromatogram, the nucleotide mixture was used (deoxyadenosine (dA), deoxyguanosine (dG), deoxycytidine (dC), thymidine (dT) and riboflavin

(dR)) since every nucleotide has different attenuation coefficient. Figure 5.4(b) shows the UV absorption spectra for the nucleotides and the riboflavin. From Figure 5.4(a) the λ_{max} are $< 207\text{nm}$ and 261nm for dA; $< 200\text{nm}$ and 254nm for dG; $< 208\text{nm}$ and 268nm for dT; $< 200\text{nm}$ and 272nm for dC; $< 224\text{nm}$ and 269nm for dR (riboflavin). After identifying each peak in the chromatogram, we were able to identify and quantify each nucleotide in the DNA sample (A, T, C, G and other things such as the riboflavin and the damage fraction (we will called here z).

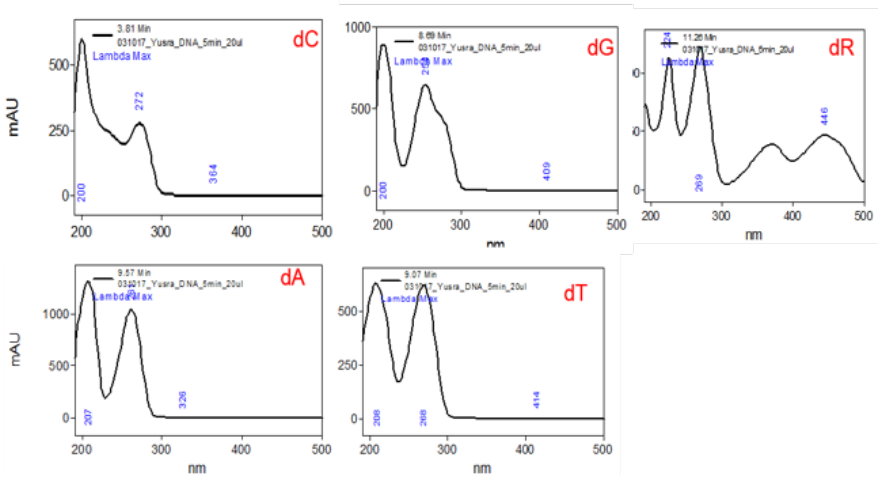

(a)

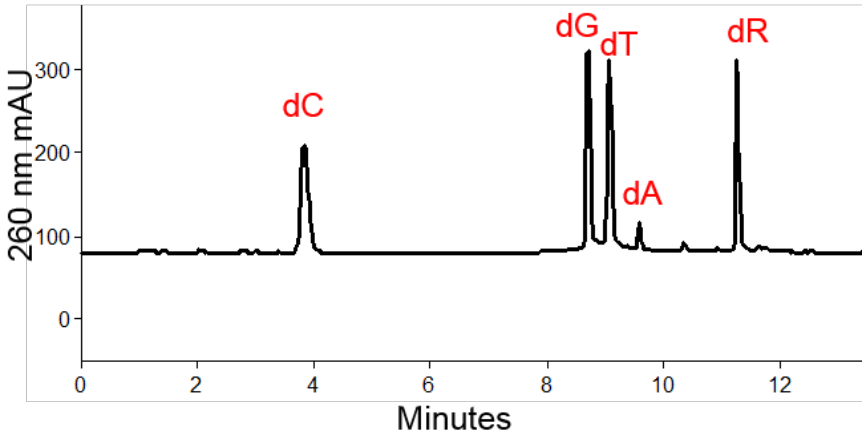

(b)

Figure 5.4: HPLC result: A) UV absorption spectra for the nucleotides and the riboflavin where (dC) Cytosine, (dA) Adenine, (dG) Guanine, (dT) Thymine, and (dR) Riboflavin. B) HPLC chromatogram of double strand DNA with riboflavin.

Figure 5.5 shows the overlapping of multiple HPLC chromotograms of the samples after irradia-

tion with UV for different times (0 min (black), 30 min (green) and 60 min (red)). From the figure below the 8.7 minute peak is dG, 9 minute is dT, 9.5 minute is dA, 11.2 minute is dR, and a unique peak (dz) is at 13.3 minute. The result shows that the amount of the uniqe peak (damage peak

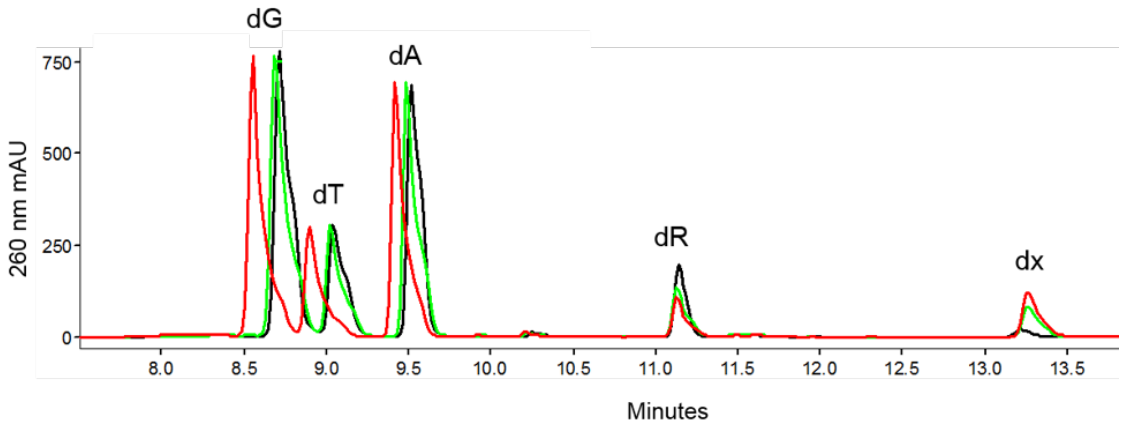

Figure 5.5: Overlapping of multiple HPLC chromatogram of the DNA nucleotides and other peaks (riboflavin and damage peak) after irradiation with UV light for different time periods ((0 min control (black), 30 min (green), and 60 min (red)). in this figure dz represent the damage peak (our interest).

dz) was increased with exposure time, while the riboflavin peak decrease with time because the riboflavin is consumed as it causes damage to the DNA. To quantify the damage fraction, the area under the peaks were integrated. The fraction was then found by dividing the unique peaks to the sum of the area of the other nucleotide. The table below shows the fraction of DNA damage for different times. The fraction of DNA damage vs exposure time was plotted and the slope (fraction

Time	0	30	60
Fraction	1.0×10^{-3}	4.6×10^{-3}	7.1×10^{-2}
Error	2.0×10^{-4}	2.7×10^{-3}	6.7×10^{-4}

Table 5.1: Fraction of the damage peaks caused by UV light for different time period

per min) was fitted, by using Origin Lab 2018 software Figure 5.6, to be $(1.00 \pm 0.192) \times 10^{-3}$.

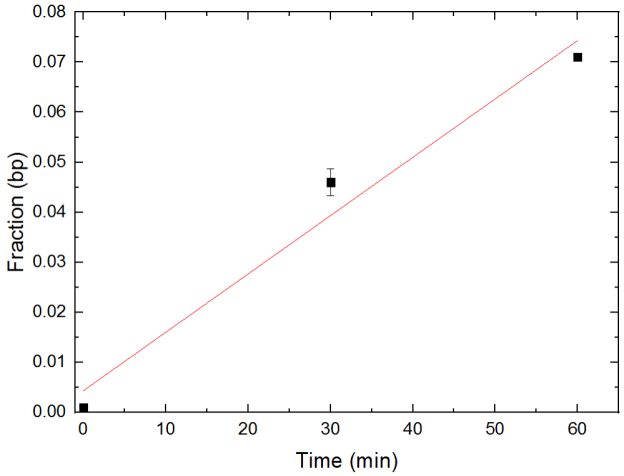

Figure 5.6: HPLC result analysis of DNA damage from UV light in the present in the riboflavin for different time period (0 min, 30min and 60 min). The slope of the line (fraction/ min) is $(1.00 \pm 0.192) \times 10^{-3}$

5.4 Conclusion

In this project we were interested in learning how to measure and quantify the DNA base damage by using the gel electrophoresis and HPLC methods. HPLC was able to give us the best estimate of the base DNA damage. In the next chapter the HPLC methods were used to quantify and measure the DNA base damage caused by different types of ionizing radiation such as gamma and proton.

Chapter 6

Measuring of the Direct DNA base Lesions Induced by High and Low LET Radiation:Using HPLC Assay

6.1 Introduction

Many studies have led to the conclusion that damage in the biological system by ionizing radiation are related to DNA damage such as strand breaks and base lesions. Unsuccessful repair of the DNA damage leads to genetic mutation or cell death. DNA damage to the base lesions is considered some of the most common damage that is caused by high energy radiation. DNA base lesions happen when one or more of the DNA bases (A, C, G and T) are chemically changed to a new form leading to harm the DNA.

Different types of radiation ionize the DNA differently. Low linear energy transfer (LET) radiation, such as gamma ray and electrons, produce sparse ionization in the DNA molecules. On the other hand, high LET radiation, such as heavy ions and low energy protons, produce ionization in a dense track along the particle path. Many studies showed that the chemical changed in the DNA bases produced by the low LET radiation are the same for the most part to those produced by high LET radiation.

In this study, we aim to analyze the DNA base modifications induced by the direct effect of low and high LET radiation. The dry plasmid DNA was irradiated to gamma radiation (low LET) and proton beam (high LET). After irradiating the samples, the DNA was digested to a single nucleotides (A, T, C, and G) and other compounds which were our interests. HPLC was then used to separate the DNA nucleotide and the other product, then the amount of the nucleotides and the product were quantified.

6.2 Gamma irradiation (low LET)

6.2.1 Method

The purified DNA sample, pUC19 double stranded plasmid (2686 base pair), was obtained from Bayou Biolabs Co. (Metairie, LA). The plasmid was predominantly in the supercoiled state, with a small amount of plasmid in the nicked state. The DNA was diluted in 10 mM Tris-Cl, 1 mM EDTA, and pH 8.0. The original concentration of DNA was $1\ \mu g/\mu l$. For the irradiation experiment, 400 μl of DNA was mixed with $2\ \mu l$ of 10% HCL, pH 7. Thirteen $10\ \mu l$ aliquots, each containing 10 μg of plasmid DNA, were pipetted into a 1.5 microcentrifuge tube. The tube samples were then divided to three groups.

1. The first group (three tubes) was used as unirradiated control.

2. The second group (five samples) were irradiated with a radiation dose of 30 Gy (low normal).

3. For the third group, five samples were irradiated with a higher radiation dose 100 Gy (high normal).

The samples were dried via a high - drying rate SpeedVac for one hour. The samples were then irradiated on a sample holder, as shown in Figure 6.1.

To irradiate the samples, the sample holder was placed inside a water tank at a 5 cm depth (Figure 6.2). Subsequently, the samples were exposed to gamma rays produced by a LINAC (NovALis, BrainLab, Munich, Germany) at Precision Radiotherapy (Cincinnati, OH) at 30 Gy (low dose) and

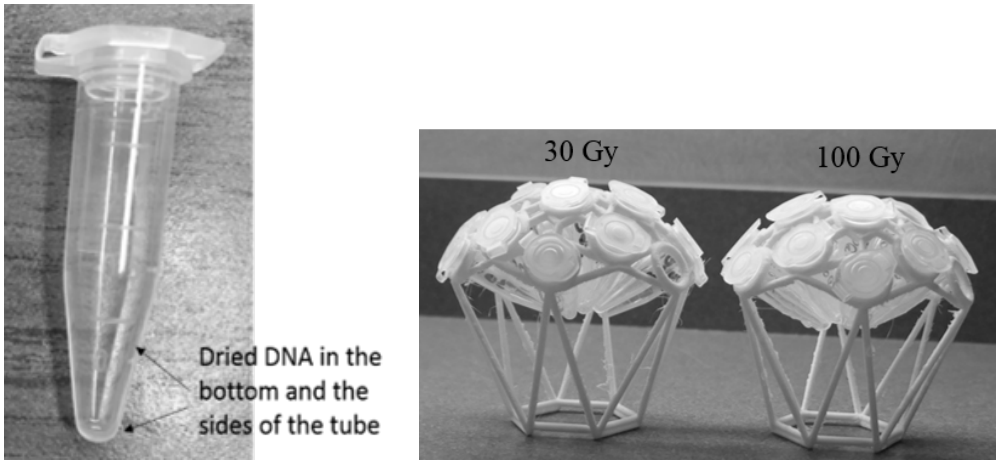

(a) (b)

Figure 6.1: Dry DNA in the 1.5 microcentrifuge tube. a) Dry samples in the bottom and the sides of the tube. b) Two of the sample holder one for low dose (30 Gy) and the other for high dose (100 Gy).

100 Gy (high dose), and the LET is $0.26\ \mathrm{keV}/\mu\mathrm{m}$. Before and after irradiation, the samples were preserved at a temperature of -20^0C. Before irradiation they were brought to room temperature.

(a) (b)

Figure 6.2: Radiation setup: a) water tank (5 cm depth) on the top of the radiation beam. b) The sample holder inside the water tank where the dry samples (in the bottom of the tube) were covered by water.

After irradiation, the DNA was digested to single nucleotides (A, T, C, and G) and other compounds. In the beginning, the samples (three samples from each group) were dissolved into $10\ \mu l$ of (40 mM Tris; 10 mM; pH 8.5). DNA digestion into nucleosides was performed by adding $1\ \mu l$ of $1\ U/\mu l$ of Calf Intestinal Alkaline Phosphatase (CIAP). Samples were then incubated for 90

min at 37^0C. Subsequently, 0.5 μl of 0.1 $U/\mu l$ snake venom phosphodiesterase was added, and the samples were incubated for 90 min at 37^0C. Then, 1 μl of 3 $U/\mu l$ of deoxyribonuclease was added, and the samples were incubated for 90 min at 37^0C. After that, 90 μl of HPLC solvent, which contained 9.75 ml of deionized water, 0.25 ml of acetonitrile and 10 μl of formic acid, was added to the samples. After digestion, An Agela technologies C18 [5 μm, 100A, 4.6 x 100mm] column, a stationary phase, was used for separation of the DNA nucleotides by linear gradient of water [solvent A contain 98% water and 2% acetonitrile, and solvent B contain 95% acetonitrile and 5% water] (mobile phase) over several minutes .The gradient was 0% solvent B for 2 min and 95% for 14min and the mobile phase delivered at a flow rate of 1ml/min. The HPLC analysis was performed during 24 min after injection. The data was quantified using a 32 karat HPLC software.

6.2.2 Result and Discussion

The aim of this study was to find the fraction (probability) of DNA base lesions per radiation dose caused by Gamma radiation. HPLC was used to measure and quantify the base lesions.

Figure 6.3 shows an example of HPLC chromatograms of the digested DNA after photon radiation. Product formation is detected by HPLC by first using C18 column (stationary phase). To identify the nucleotides of this reaction, controls were used. The 2.9 minute peak is dC, 7.7 minute is dG, 8 minute is dT, 8.6 minute is dA, and a unique peak is at 1.6 minute. The change in the flow rate causes changes of the retention time. From Figure 6.3, we observed the fraction of the unique peak increases with radiation dose.

Three samples of each group were analyzed. The analysis is accomplished by integration of both nucleotide (A, G, C and T) peak areas and product peak areas while monitoring the absorbance at 260 nm. After the average was taken, the fraction of DNA damage rate was found by dividing the average of the unique peak by the sum of the averages of the nucleotide peaks. The measured fraction of base lesions was plotted as a function of the dose as shown in Figure 6.4.

A linear increase in the fraction as a function of radiation dose was observed for doses ranging

from 0 to 100 Gy by using Origin Lab 2018 software (Figure 6.4). The probability (fraction) per dose (Gy) was fitted to be $(1.38 \pm 0.15) \times 10^{-4}$.

Dose	0	30	100
Fraction	1.43×10^{-2}	1.69×10^{-2}	2.78×10^{-2}
Error	2.41×10^{-3}	1.18×10^{-3}	3.25×10^{-4}

Table 6.1: The fraction of DNA base damage for different radiation dose

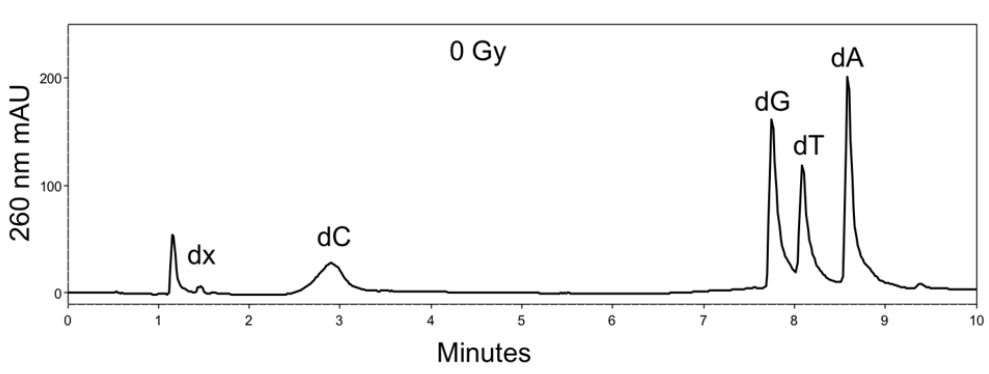

(a)

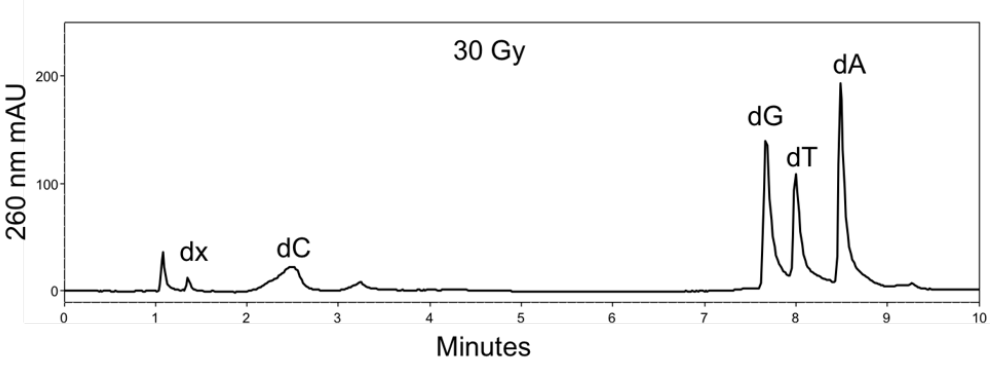

(b)

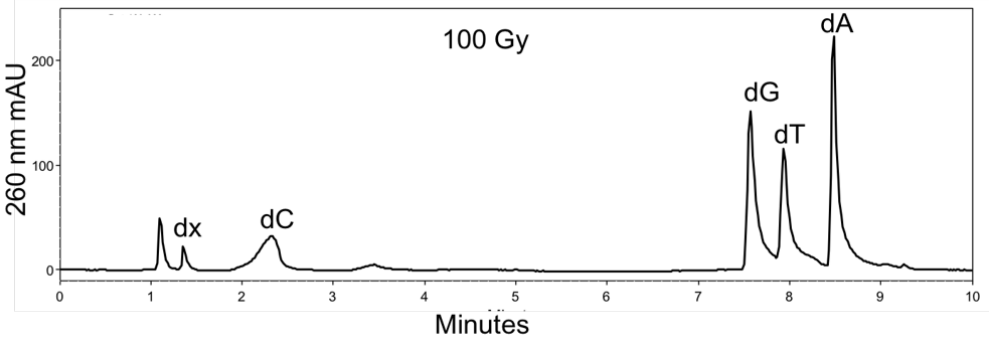

(c)

Figure 6.3: HPLC chromatogram of control (a), low radiation (b) and high radiation (c).

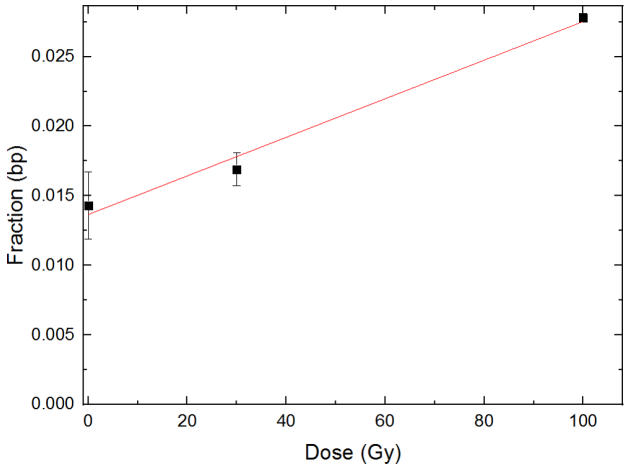

Figure 6.4: Fraction of DNA damage per bp caused by photon radiation as a function of dose (0 Gy, 30 Gy and 100Gy) detecting by use the C18 column. The slope of the line was found to be $(1.38 \pm 0.15) \times 10^{-4}$.

6.3 Proton beam irradiation

6.3.1 Method

The samples were prepared by drying down $720\ \mu l$ of DNA (pUC19). Then $720\ \mu l$ of water and 720 of HCL solution, which contain $717.57\ \mu l$ of water and $2.43\ \mu l$ of (1 M Hcl), was added to the dry DNA, pH 7. Nine $80\ \mu l$ aliquots, each containing $40\ \mu g$ of plasmid DNA, were pipetted into a 1.5 microcentrifuge tube. The tube samples were then divided to three groups. The first group had three tubes used as unirradiated control, the second group had three samples irradiated with a low- radiation dose of 30 Gy (low normal), and the third group had three samples irradiated with a high radiation dose of 100 Gy (high normal). The samples were dried via a high - drying rate SpeedVac for four hours. The samples were then irradiated to the proton beam (Cincinnati Children's Hospital Medical Center) on a sample holder, as shown in Figure 6.5.

After irradiation, the samples were dissolved into $26\ \mu l$ of buffer solution. The DNA was then digested to a single nucleotide (A, T, C, and G) and other compound by using same digestion enzymes in section 6.2.1 but different amount was used since the concentration of the DNA is different. We added $1.60\ \mu$l of $1\ \mathrm{U}/\mu$l of Calf Intestinal Alkaline Phosphatase (CIAP) ,$10\ \mu$l of 4

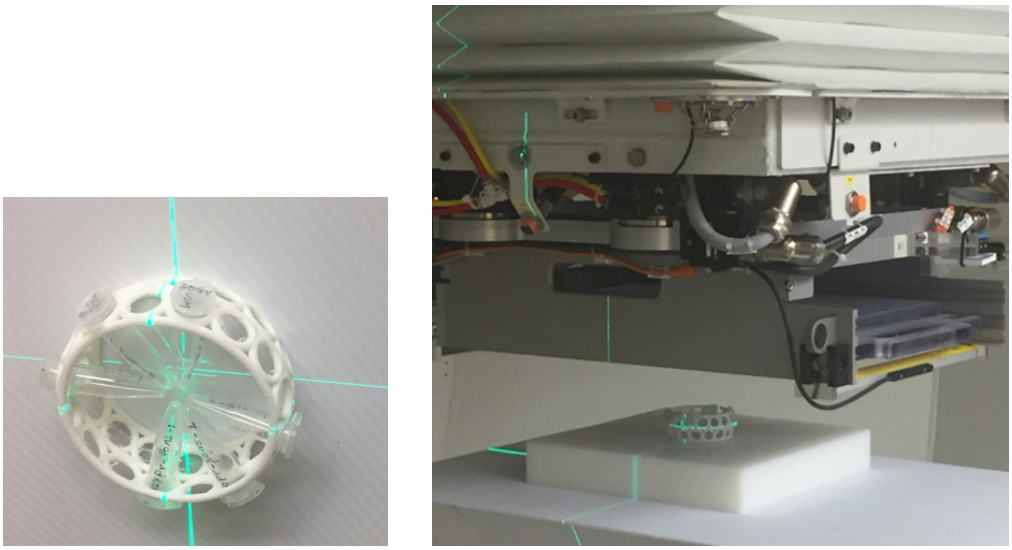

(a) (b)

Figure 6.5: Radiation setup: a) sample holder. b) Irradiated sample by the proton beam where the beam direction from the top.

$\mathrm{U/ml}$ snake venom phosphodiesterase, and 2.64 μl of 3 $\mathrm{U}/\mu\mathrm{l}$ of deoxyribonuclease . The samples were incubated overnight at 37^0C. After digestion, 100 μl of ultrapure water was added to each tube. Then an Agela technologies C18 [5um, 100A, 4.6 x 100mm] column, a stationary phase, was used for separation of the DNA nucleotides with the same gradient as in section 6.2.1. The HPLC analysis was performed for 24 min after injection.

To get more separation, we used different (stationary phase) for more sensitive result. To do this, the samples were dried via a high - drying rate SpeedVac overnight. Then, the samples were dissolved into 100 μl of (95% of ACN and 0.1% formic acid). Then the samples was run through HPLC by using different type of column (Amid column) which produce more sensitive result.

6.3.2 Result and Discussion

The goal of this study was to quantify and measure the DNA base lesions induced by a proton beam (high LET radiation) by using HPLC methods. After the DNA was irradiated and digested, different types of HPLC column were used to detect the DNA base lesions.

The first column was C18, which was used before to detected base damage induced by gamma radiation (section 6.2.1). Three samples of each group were analyzed. The analysis was accom-

plished by integration of both nucleotide (A, G, C and T) peak areas and product peak areas while monitoring the absorbance at 260 nm. After the average was taken, the fraction of DNA damage was found by dividing the average of the unique peak by the sum of the averages of the nucleotide peaks (Table 6.2). The measured amount of fraction of DNA lesions were plotted as a function of the dose as shown in Figure6.6. A linear increase in the fraction of DNA damage, as a function of radiation dose, was observed for doses ranging from 0 to 100 Gy. The probability (fraction) per dose (Gy) was fitted to be about $(0.14 \pm 0.17) \times 10^{-4}$.

Column type	Dose (Gy)	Damage fraction per bp	Error
C18	0	6.19×10^{-3}	9.19×10^{-4}
	30	4.87×10^{-3}	4.34×10^{-4}
	100	7.19×10^{-3}	1.90×10^{-3}
Amid	0	6.93×10^{-2}	1.12×10^{-2}
	30	6.25×10^{-2}	9.94×10^{-3}
	100	1.13×10^{-1}	2.51×10^{-2}

Table 6.2: The fraction of DNA base damage for different radiation dose. Different type of column was used (C 18 and Amid).

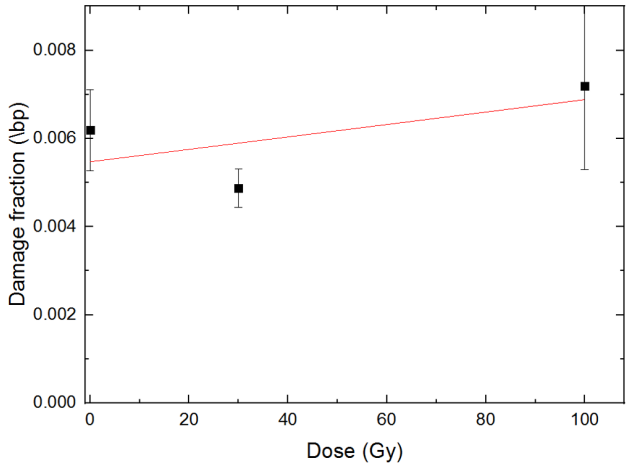

Figure 6.6: Fraction of DNA damage per bp caused by proton beam as a function of dose (0 Gy,30 Gy and 100 Gy) detecting by use the C18 column. The slope of the line was found to be $(1.41 \pm 1.77) \times 10^{-5}$

The second type of the HPLC column is amid column and this type of column produces high sensitivity separation. Figure 6.7 shows an example of overlapping HPLC chromatograms (control (blue), low dose 30 Gy (red) and high dose 100 Gy (Green)) of the digested DNA after proton

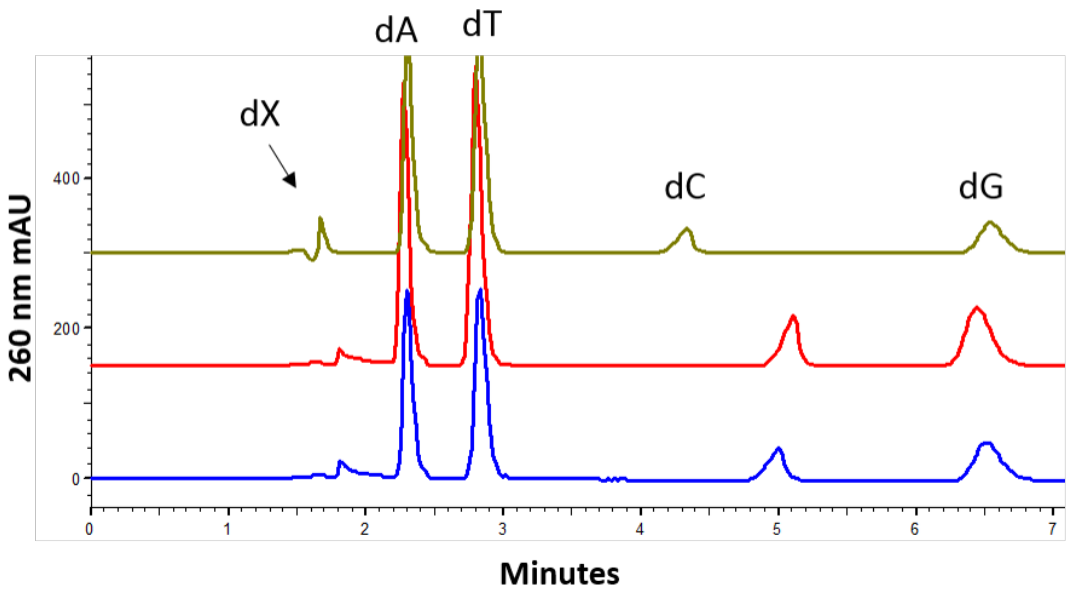

Figure 6.7: The HPLC chromatogram of DNA nucleotide and the damage peak after proton beam after using amid column. Control (blue), low radiation dose (30 Gy) (red) and high radiation dose (100 Gy) (green).

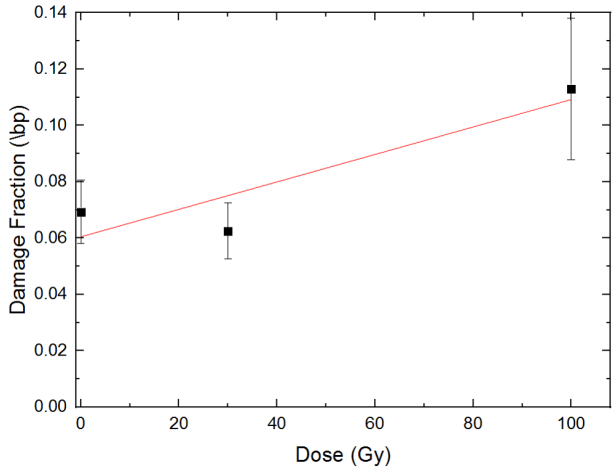

Figure 6.8: Fraction of DNA damage per bp caused by proton beam as a function of dose (0 Gy, 30 Gy and 100 Gy) detecting by use the Amid column the slope of the line is $(4.87 \pm 2.18) \times 10^{-4}$

radiation. The DNA nucleotides and other products were detected by HPLC by using amid column (stationary phase). To identify the nucleotides of this reaction, controls were used. The 2.3 minute peak is dA, 2.8 minute is dT, 5 minute is dC, 6.5 minute is dG, and a unique peak (dX) is at 1.8 minute. The change of the flow rate causes changes of the retention time. From Figure 6.7, we found that the fraction of the unique peak (dX) increases with radiation dose. The probability

(fraction) per dose (Gy) was estimated to be about $(4.87 \pm 2.18) \times 10^{-4}$ (Figure 6.8).

6.4 Conclusion

In this study, we aimed to find the fraction of DNA base lesions per unit dose caused by direct effects of high and low LET radiation by using a direct method HPLC. Dry DNA samples were irradiated to gamma ray (low- LET) and to proton beam (high LET). Then, HPLC were used to separate DNA samples to single nucleotides and to quantify them.

From the result we found that the fraction of DNA base modified per Gy for high LET radiation is lower than the fraction of DNA base lesions per Gy caused by gamma.

Chapter 7

Application of the Track Model to Published Results on Nucleotide Base Modifications

7.1 Introduction

Interacting charged particles with DNA causes ionization (holes) to the DNA strands. These holes may be locally clustered leading to various type of DNA damage such as single-strand breaks, double-strand breaks, and base lesions. Based on the track model, the cluster size which is the number of holes j per cluster and the cluster length r_0 which is the distance scale for clustering of holes in the cluster may correlate with the damage rate and complexity. In our model, we choose the r_0 for DNA base modification to be 0.34 nm (approximate size of the nucleotides) and then we tested the model for different r_0 values to see how the model rate predictions depend on r_0. In this chapter, we compared the track model with experimental measurements of DNA base lesions to estimate the effective value of r_0 and j for nucleotides lesions.

7.2 Applying the track model to nucleotide base lesions measured by HPLC

7.2.1 Rate of DNA base modification induced by carbon ion

Analysis of published experimental data

The rates of formation for eight different DNA base lesions caused by low and high LET radiation were measured by (Pouget et al ,2002) [9]. The THP-1 cell line – a type of human white blood cell- was exposed to gamma ray and Carbon ions. For low LET radiation, gamma rays were produced by a ^{60}C source and samples were exposed to a dose range from 90 to 450 Gy. The LET is 0.26 $keV/\mu m$. Other samples were exposed to carbon ions with a dose range from 100 to 1000 Gy. The LET is 25 $keV/\mu m$, which is 100-fold higher than the LET of the gamma ray. Then, the DNA was extracted from the cell and digested to single nucleotides. The cellular DNA base damages were measured by using HPLC-MS/MS assay. The effect of Gamma radiation compared with Carbon ion radiation on the yield of the six DNA base lesions (thymidine glycols, 8-oxodAdo, 8-oxodGuo, FapyGua, 5-HmdUrd,and 5-FordUrd) are shown in Table 7.1. The uncertainty of the yield that was found by Pouget was not given in the paper. We estimated it by replotting the rates shows in a tables in the paper by using Origin Lab 2018 software. Figure 7.1 shows the replotting result of Thymidine glycols, and the other remaining base lesions are shown in Figure A.-1. In Table 7.1,

DNA base lesions	Yield/Mbp/Gy Gamma ray	Yield/Mbp/Gy Carbon ion	Ratio (R) of Carbon/Gamma
Thymidine glycols	$(9.7 \pm 0.65) \times 10^{-2}$	$(6.2 \pm 0.59) \times 10^{-2}$	0.639 ± 0.074
8-oxodAdo	$(3.6 \pm 0.80) \times 10^{-3}$	$(2.6 \pm 0.29) \times 10^{-3}$	0.722 ± 0.180
8-oxodGua	$(2.0 \pm 0.10) \times 10^{-2}$	$(0.96 \pm 0.06) \times 10^{-2}$	0.48 ± 0.038
FapyGua	$(4.3 \pm 0.50) \times 10^{-2}$	$(2.2 \pm 0.04) \times 10^{-2}$	0.512 ± 0.062
5-HmdUrd	$(2.9 \pm 0.49) \times 10^{-2}$	$(1.3 \pm 0.10) \times 10^{-2}$	0.448 ± 0.083
5-FordUrd	$(2.2 \pm 0.22) \times 10^{-2}$	$(1.1 \pm 0.10) \times 10^{-2}$	0.500 ± 0.067

Table 7.1: The yield of formation of six DNA base lesions induced by Gamma ray and Carbon ion (Pouget et al.,2002). The error of the yield was found by fitting the data by using Origin Lab 2018 software.

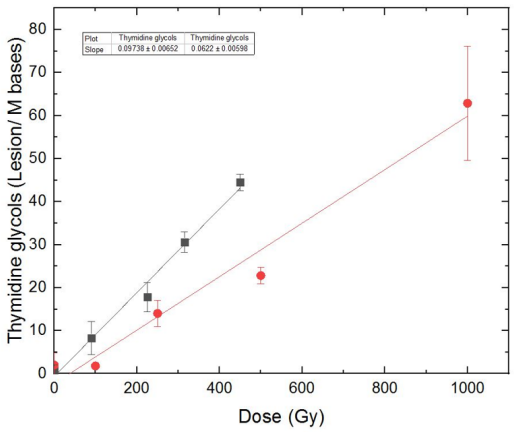

(a)

Figure 7.1: Gamma- radiation induced and Carbon -ion induced formation of Thymidine glycols (circle) Carbon- ion (Pouget et al. 2002). The data was fitted by using origin lab 2018 software . The slopes with the uncertainty of the base lesions was found by using the origin software.

the ratio R of the DNA lesions yields caused by carbon ions compared with gamma ray with the uncertainties δR was calculated by using the equation below:

$$\delta R = |R| \sqrt{\frac{\delta X}{X}^2 + \frac{\delta Y}{Y}^2} \tag{7.1}$$

where X is the yield of base lesions caused by gamma radiation with the uncertainty δX, and Y is the yield of base lesions caused by carbon ion with the uncertainty δY.

The weighted mean μ of the ratios of the lesions yields between Carbon to Gamma R_i that have error a was then estimated by using the equation below

$$\mu = \frac{\sum R_i / {a_i}^2}{\sum 1/{a_i}^2}$$

Where i is the DNA base lesions. And the error on the weighted mean a is

$$\sqrt{a^2} = \sqrt{\frac{1}{\sum 1/{a_i}^2}}$$

The weighted mean was estimated to be 0.509 ± 0.025 .

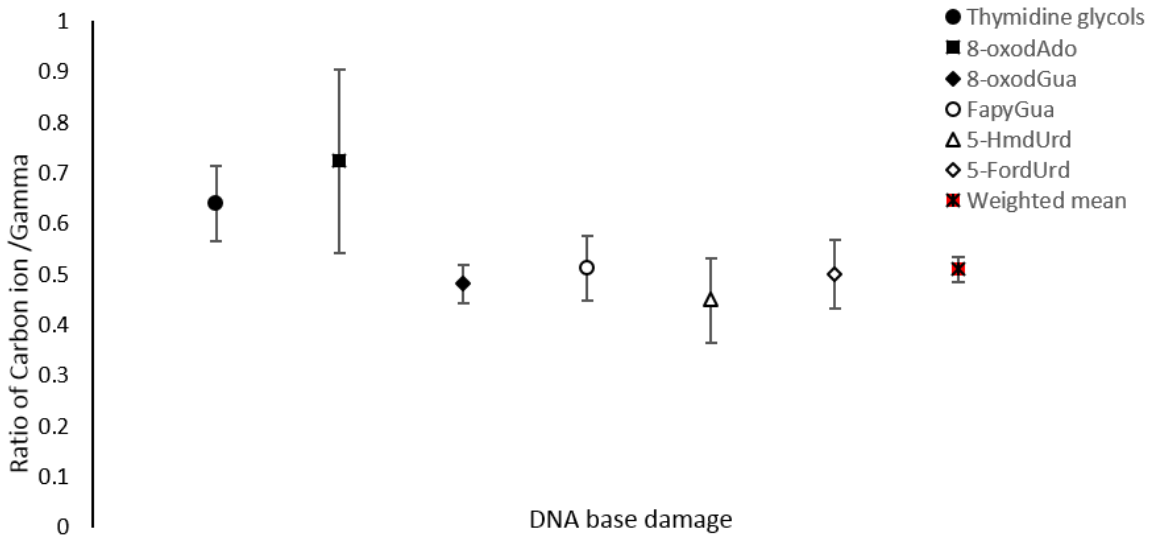

Figure 7.2: The ratio of the DNA lesions yields caused by carbon compared to gamma for six DNA base lesions and the weighted mean.

Result and Discussion

The result from Pouget shown the yields of DNA base lesions obtained with Carbon ion (high LET) are lower than the yields with Gamma ray (low LET) by a factor of ≈ 2 . In this section, we aim to explain these result by comparing the experimental result with the track model. The ratio between high LET $25\ keV/\mu m$ to low LET $0.26\ keV/\mu m$ with complexity index ≥ 1, 1, 2 and 3 in the track model was found (Table 4.5).

The weighted mean of the ratios between high LET to low LET of the six of DNA base lesion was then compared with the ratio between high LET to low LET in the track model (Figure 7.3). From Figure 7.3, we concluded that the six base modifications studied are consistent with single ionization and likely do not involve clustered ionization.

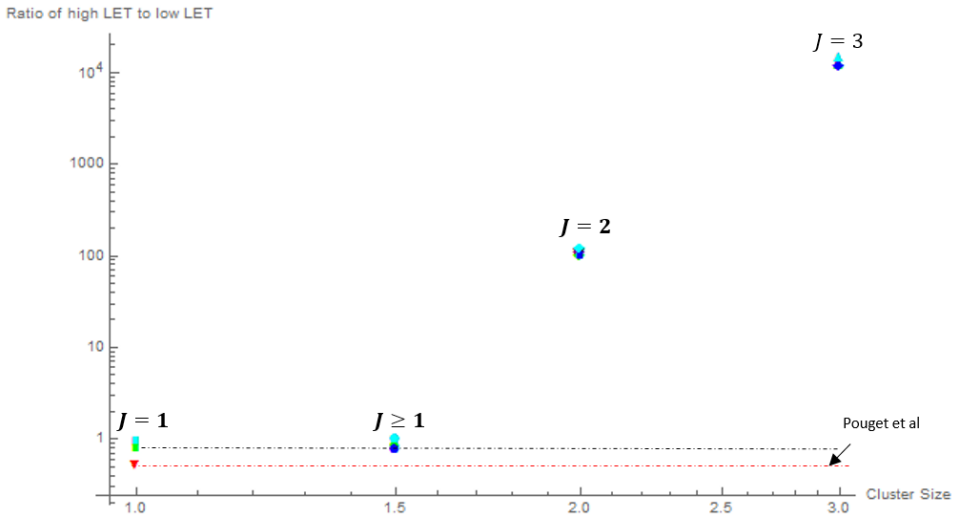

(a)

Figure 7.3: Examination of the ratio of the rate of base lesions caused by carbon ion to gamma ray that was measured by (Pouget et al., 2002) with the ratio of high LET to low LET in the track model for different r_0 values (0.2 nm (cyan), 0.34 nm (black), 0.5nm (purple), 0.8nm (green) and 1nm (blue)) for different cluster size (complexity).The error of the rate of base lesion is small.

7.3 Fitting of the track model to nucleotide base lesions measured by gel electrophoresis

7.3.1 Rate of DNA base modification induced by various charged particles

Analysis of published experimental data

The yield of nucleobase lesion in dry plasmid DNA (pUC18, $2686\ bp$), irradiated with various charged particles, was measured by (Ushigome et al, 2012)[12] and (Urushibara et al,2007) [11]. The DNA base lesions were quantified by using the base excision repair enzymes such as endonuclease III (Nth) to detect T and C base lesions and formamidopyramidine DNA glycosylase (Fpg) to detect G, A base lesions. These enzymes are able to identify damaged bases from the DNA helix and remove them by creating an additional break in the strand of DNA. These breaks can be measured by using gel electrophoresis. By subtracting the rate of prompt DNA strand breaks from the rate of breaks caused by the excision enzymes, the rate for base lesions can be quantified.

Tables 7.3 and 7.2 show the yield of base lesions induced in DNA by charged particles for several values of LET. The results in the published table were converted from $SSB/Gy/Da$ to $SSB/Gy/Mbp$ by multiplying the result values by average molecular weight of double strand DNA base pairs $650\ g/mol$.

The error on the yield of base lesions that was found by (Urushibara et al. , 2007) was not given in the paper. However, the error of the yields of SSB (prompt damage)(δx) and the error of the yields of SSB with the additional single strand breaks caused by the enzymes ($SSB_{Nth\&Fpg}$)(δy) are shown (Table 7.2)[11].

LET ($keV/\mu m$)	SSB/Gy/Mbp	$SSB_{Nth\&Fpg}$/Gy/Mbp	Base lesion/Gy/Mbp
0.26	$(4.36 \pm 0.52) \times 10^{-2}$	$(15.6 \pm 1.1) \times 10^{-2}$	$(11.2 \pm 1.2) \times 10^{-2}$
19	$(4.88 \pm 0.97) \times 10^{-2}$	$(18.7 \pm 2.0) \times 10^{-2}$	$(13.8 \pm 2.2) \times 10^{-2}$
63	$(4.75 \pm 0.65) \times 10^{-2}$	$(12.5 \pm 1.6) \times 10^{-2}$	$(7.74 \pm 1.70) \times 10^{-2}$
95	$(4.36 \pm 0.26) \times 10^{-2}$	$(8.06 \pm 0.65) \times 10^{-2}$	$(3.71 \pm 0.70) \times 10^{-2}$
121	$(2.93 \pm 0.32) \times 10^{-2}$	$(6.24 \pm 0.78) \times 10^{-2}$	$(3.32 \pm 0.80) \times 10^{-2}$
148	$(2.47 \pm 0.13) \times 10^{-2}$	$(3.38 \pm 0.26) \times 10^{-2}$	$(9.10 \pm 2.90) \times 10^{-3}$

Table 7.2: Yields of SSB and $SSB_{Nth\&Fpg}$ induced in plasmid DNA by high and low LET radiation. The result by (Urushibara et al. , 2007) is calculated in SSB/Gy/Da and it is converted to SSB/Gy/Mbp the uncertainty was given.

After subtracting the yield of the prompt damage from $SSB_{Nth\&Fpg}$, we estimated the error,δR, (Table 7.2) by using equation below

$$\delta R = \sqrt{(\delta x)^2 + (\delta y)^2} \tag{7.2}$$

where δx is the uncertainty on the yield of SSB (prompt damage) and δy the yield of $SSB_{Nth\&Fpg}$.

Also, the yield of base lesions found by (Ushigome et al , 2012) was recalculated (Table 7.3) (same as above) to be a consistent in method with Urushibara.

To fit the data, we used least squares curve fitting on the rates in Tables 7.2 and 7.3 with the track model curves. The equation (4.6) was used for data fitting. For DNA base lesion we assume that $j = 1$ or $j \geq 1$. The equation was multiplied by a fitting parameter (a) which represents an efficiency. We aim to find the value of the parameter r_0 that best describes the data (Table 7.4).

LET ($keV/\mu m$)	SSB/Gy/Mbp	$SSB_{Nth\&Fpg}$/Gy/Mbp	Base lesion/Gy/Mbp
2.2	$(5.79 \pm 1.50) \times 10^{-2}$	$(19.6 \pm 4.4) \times 10^{-2}$	$(13.7 \pm 2.6) \times 10^{-2}$
6	$(6.24 \pm 1.17) \times 10^{-2}$	$(23.2 \pm 6.7) \times 10^{-2}$	$(17.0 \pm 4.9) \times 10^{-2}$
13	$(9.88 \pm 2.41) \times 10^{-2}$	$(32.4 \pm 6.1) \times 10^{-2}$	$(22.5 \pm 5.1) \times 10^{-2}$
31	$(9.56 \pm 2.28) \times 10^{-2}$	$(24.3 \pm 5.3) \times 10^{-2}$	$(14.8 \pm 2.6) \times 10^{-2}$

Table 7.3: Yields of SSB and $SSB_{Nth\&Fpg}$ induced in plasmid DNA by high and low LET radiation. The result by (Ushigome et al , 2012) is calculated in SSB/Gy/Da and it is converted to SSB/Gy/Mbp the uncertainty was given.

Figures 7.4 (a), 7.5 (a),7.8 (a) and 7.7 (a) show the fitted curves. To estimate the goodness of fit, we calculated the chi square (χ^2) by summing the ratios of the residual to error for each data point (Figures 7.4 (b) , 7.5 (b) ,7.8 (b) and 7.7 (b)) .

$$\chi^2 = \sum (\frac{residual_i}{\sigma_i})^2 \tag{7.3}$$

Since the fitting curve that we select has two parameters (a,r_0), we found the degree of freedom DOF by subtracted number of data points from the number of parameters (Table 7.4).

	J	a	$r_0\ nm$	χ^2	χ^2/DOF
Ushigome	1	2.50 ± 0.31	1.60 ± 0.15	5.17	0.86
	≥ 1	2.65 ± 0.56	7.02 ± 1.92	21.90	3.65
Urushibara	1	1.55 ± 0.13	1.22 ± 0.10	13.81	3.45
	≥ 1	0.10 ± 0.001	3.90 ± 0.65	25.15	6.28

Table 7.4: Chi square χ^2 fit to the two sets of data ((Urushibara et al. , 2008) and (Ushigome et al , 2012).

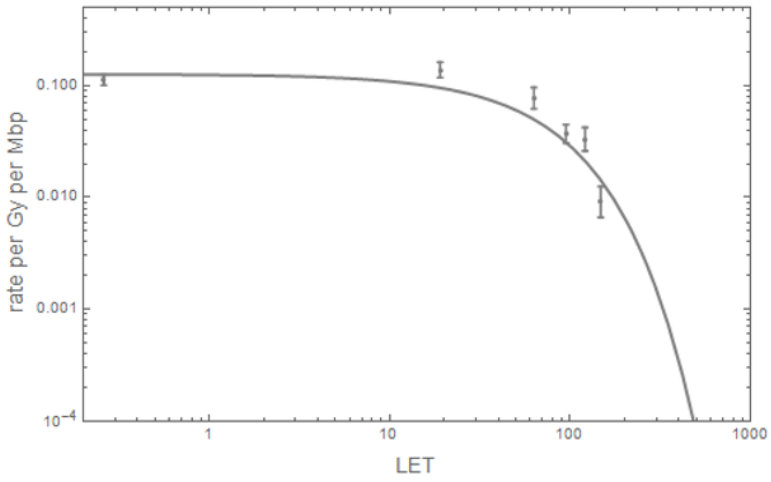

(a)

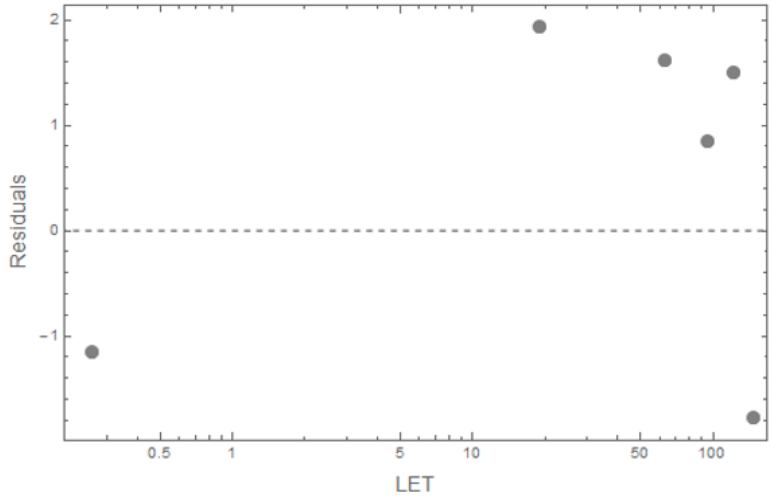

(b)

Figure 7.4: The yield of DNA base lesions caused by irradiating dry DNA with charged particles for several values of LET (Urushibara et al., 2007). a) Fit of the data with the clustering function when $j = 1$ the r_0 value is 1.22 ± 0.10 nm . b) The ratio of the residual to error vs the LET at $j = 1$. Data were fitted by using Mathematica 10.

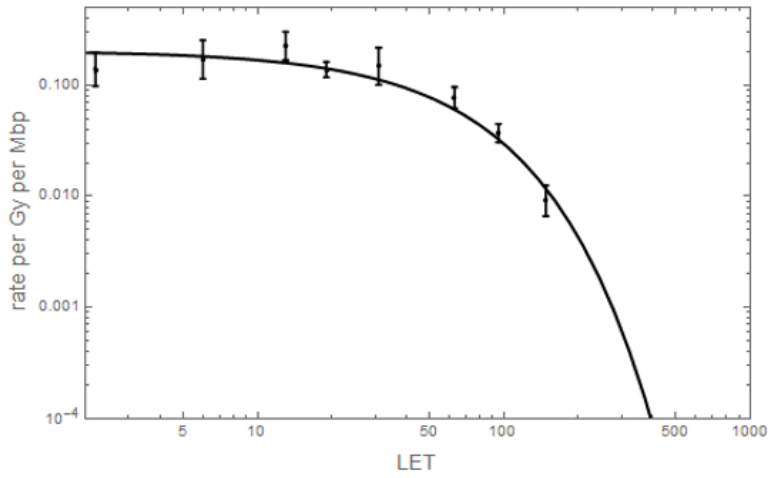

(a)

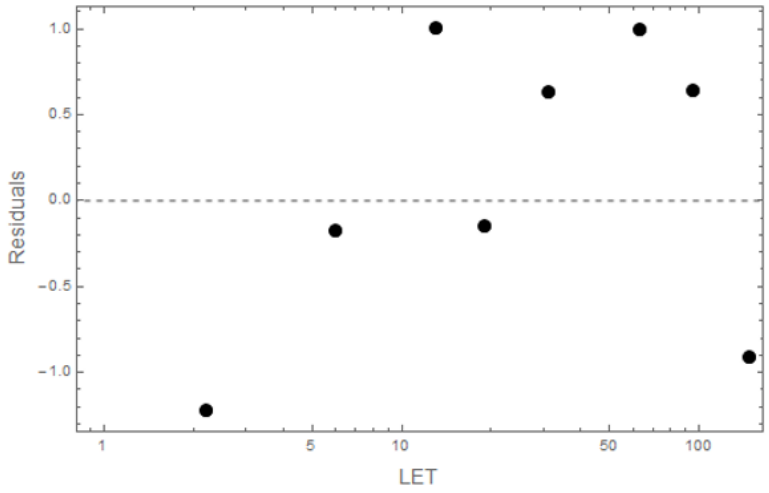

(b)

Figure 7.5: The yield of DNA base lesions caused by irradiating dry DNA with charged particles for several values of LET (Ushigome et al., 2012) (some data points 19, 63, 95 and 148 $keV/\mu m$ were used from (Urushibara et al. , 2007)) . a) Fit of data points with fitted curve with the clustering function when $j = 1$ the r_0 value is 1.60 ± 0.15 nm . b) The ratio of the residual to error vs the LET at $j = 1$.Data were fitted by using Mathematica 10.

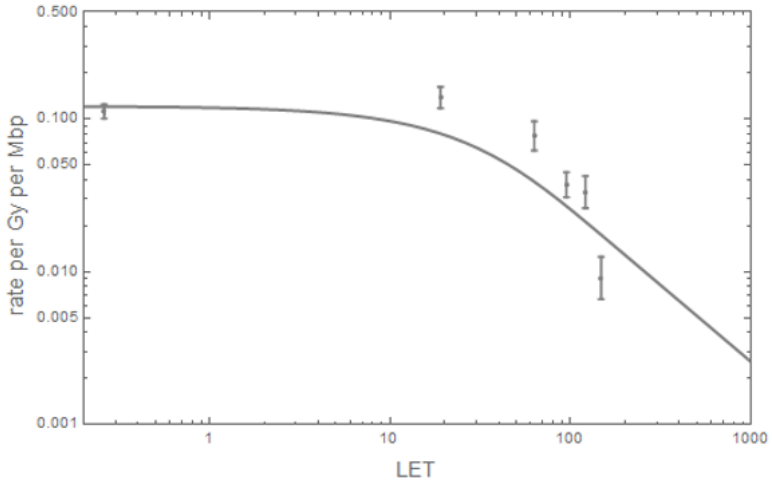

(a)

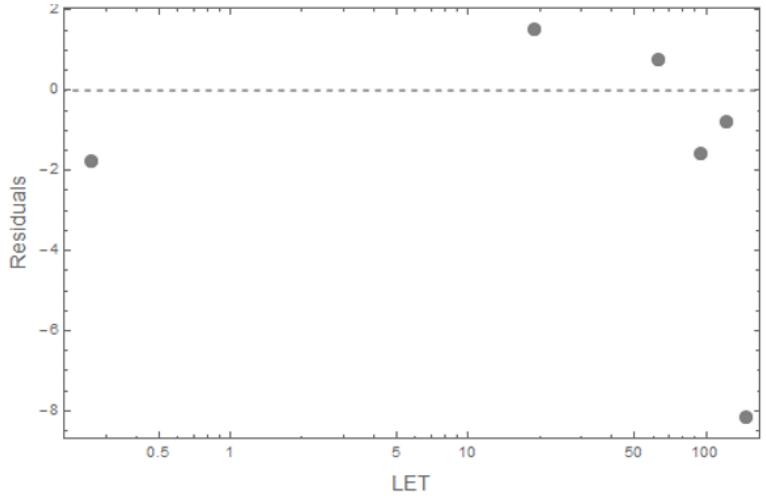

(b)

Figure 7.6: The yield of DNA base lesions caused by irradiating dry DNA with charged particles for several values of LET (Urushibara et al., 2007). a) Fit of the data points with fitted curve with the clustering function when $j \geq 1$ the r_0 value is 3.90 ± 0.65 nm . b) The ratio of the residual to error vs the LET at $j \geq 1$. Data were fitted by using Mathematica 10.

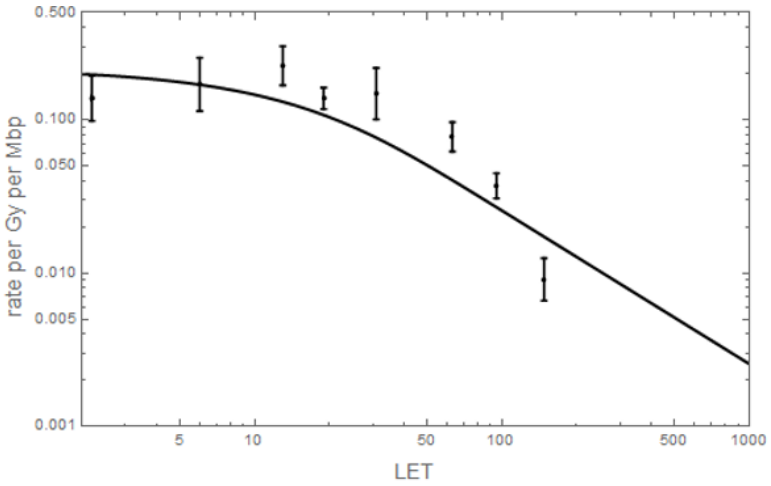

(a)

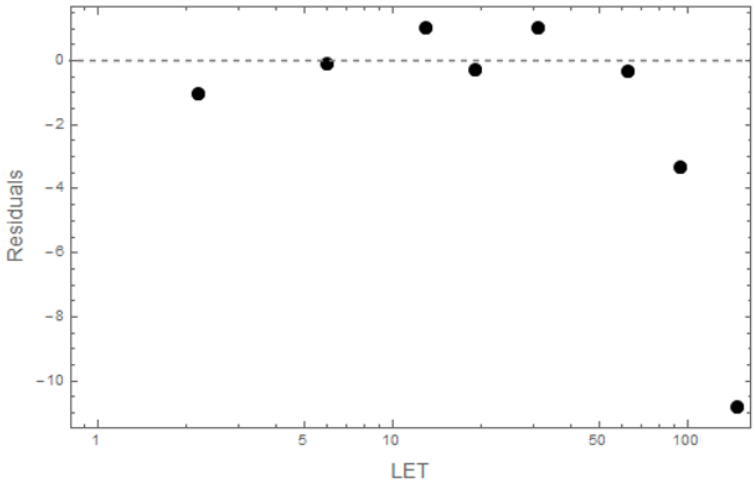

(b)

Figure 7.7: The yield of DNA base lesions caused by irradiating dry DNA with charged particles for several values of LET (Ushigome et al., 2012) (some data points 19, 63, 95 and 148 $keV/\mu m$ were used from (Urushibara et al. , 2007)). a) Fit of the data points with fitted curve with the clustering function when $j \geq 1$ the r_0 value is 7.02 ± 1.92 nm . b) The ratio of the residual to error vs the LET at $j \geq 1$. Data were fitted by using Mathematica 10.

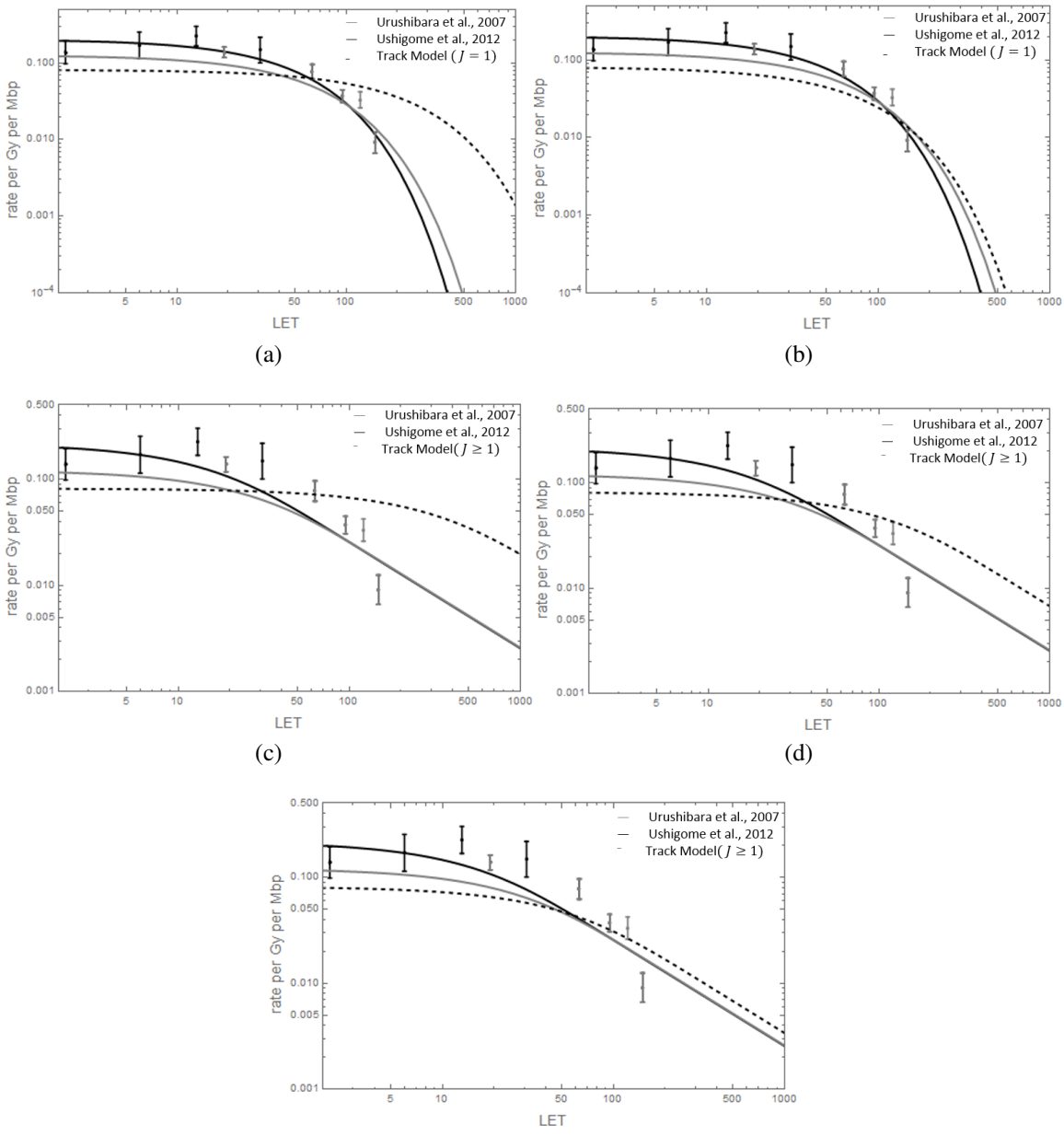

Figure 7.8: Comparison of fits to the yield of the DNA base lesions in dry DNA by charged particles vs LET (Urushibara et al., 2007) and (Ushigome et al., 2012) with the track model. Colors are shown for fits to Ushigome (black), Urushibara (gray) and the track model(dashed black line). For a) the $r_0 = 0.34$ nm , $j = 1$. b) $r_0 = 1$ nm ,$j = 1$. c) $r_0 = 0.34$nm , $j \geq 1$. d) $r_0 = 1$nm , $j \geq 1$. e) $r_0 = 2$ nm , $j \geq 1$. Data were fitted by using Mathematica 10.

Result and Discussion

The rate of DNA base modification caused by high LET radiation compared with the track model at $j = 1$ and $j \geq 1$ (Figure 7.8). Figures 7.8 (a) and (b) show the experimental data (Ushigome (black), Urushibara (gray)) with curves for fits with the track model (dashed black line). The r_0 for the fitted result is $\approx 1\mathrm{nm}$ for $j = 1$ (Figure 7.8) (a) and $\approx 3\mathrm{nm}$ for $j \geq 1$ (Figure 7.8) (b).
For $j \geq 1$, the fit is not good because the value of the Chi-square (which represent the goodness of the fit) is high (Table 7.4). Thus, we concluded that the result follows $j = 1$.

7.4 Conclusion

In this chapter, we aim to find the appropriate cluster scale and cluster size that correlate to DNA base lesion in the track model. The yield of DNA base lesions caused by low and high LET radiation was compared with the track model. By using measurement data from various methods, we can concluded that the DNA base modification is from single ionization ($j = 1$) and not from complex DNA lesions.

Appendices

Appendix A

Analysis of Pouget Result

A.1 Fit result by Origin Lab software 2018 (plot)

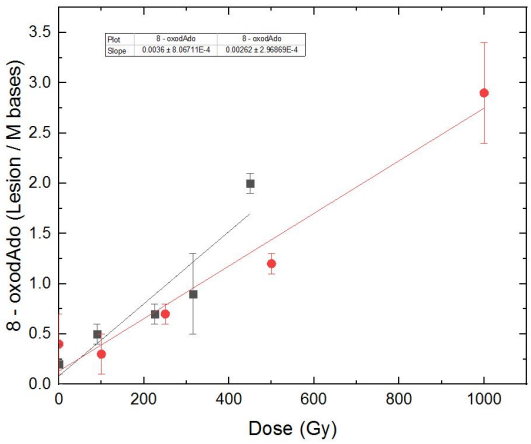

(a)

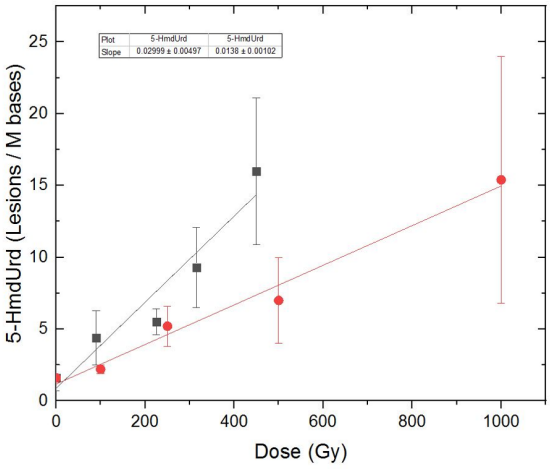
Plot 5-HmdUrd 5-HmdUrd
Slope 0.02999 ± 0.00497 0.0138 ± 0.00102
5-HmdUrd (Lesions / M bases)
Dose (Gy)
0
5
10
15
20
25
0
200
400
600
800
1000

(b)

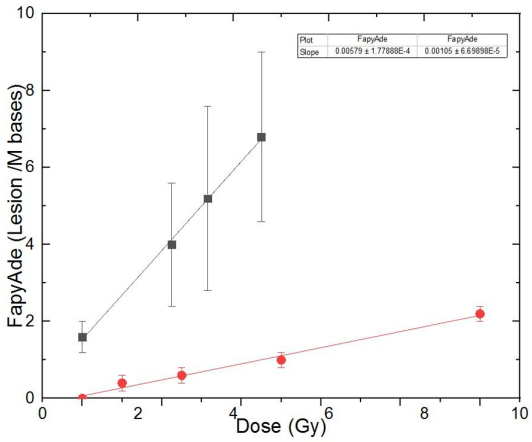
Plot FapyAde FapyAde
Slope 0.00579 ± 1.77888E-4 0.00105 ± 6.69898E-5
FapyAde (Lesion /M bases)
Dose (Gy)
0
2
4
6
8
10

(c)

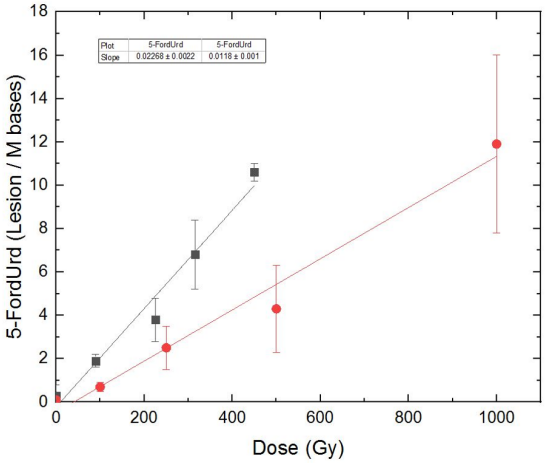
Plot 5-FordUrd 5-FordUrd
Slope 0.02268 ± 0.0022 0.0118 ± 0.001
5-FordUrd (Lesion / M bases)
Dose (Gy)
0
2
4
6
8
10
12
14
16
18
0
200
400
600
800
1000

(d)

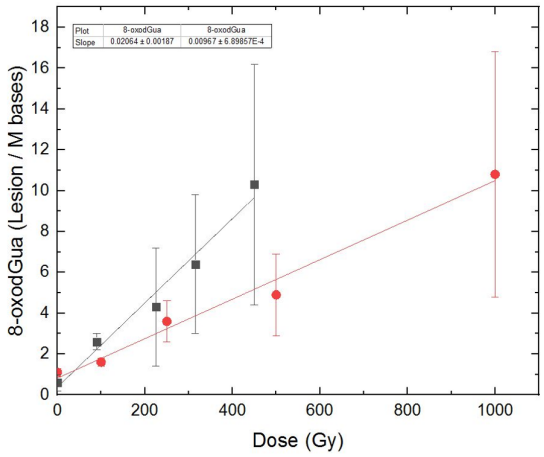

(e)

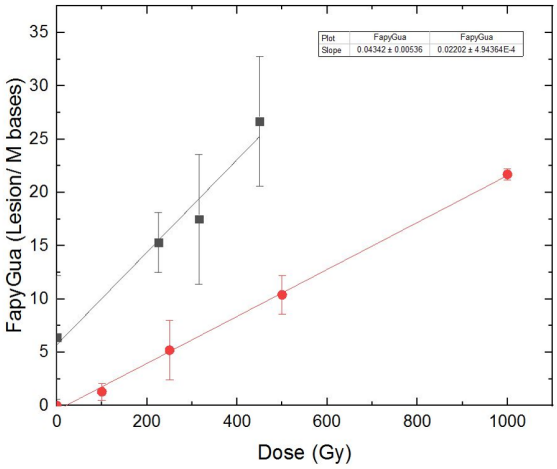

(f)

Figure A.-1: Data from (Pouget et al 2002) was fitted by using origin lab 2018 software. Gamma-radiation- induced and Carbon -ion Induced formation of eight of DNA base lesion: (square) Gamma radiation; (circle) Carbon- ion. The slopes with the uncertainty of the eight base lesions was found by using the origin software. a) 8-oxodAdo. b) 5-HmdUrd. c) FapyAde. d) 5-FordUrd. e) 8-oxodGua. f) FapyGua.

References

[1] S. P. Ahlen. Theoretical and experimental aspects of the energy loss of relativistic heavily ionizing particles. *Rev. Mod. Phys.*, 1980.

[2] J. M. Berg, J. L. Tymoczko, and L. Stryer. *Biochemistry*. W.H. Freeman Company, 2015.

[3] K. H. Chadwick and H. P. Leenhouts. *The molecular theory of radiation biology*. Springer-Verlag, 1980.

[4] J. Clark. High performance liquid chromatography - hplc.

[5] Hall E. J. and A. J. Giaccia. *Radiobiology for the radiologist*. Wolters Kluwer Health/Lippincott Williams Wilkins, 2012.

[6] J. Kiefer. *Biological radiation effects*. Springer-Verlag, 1989.

[7] V. Kumar, O. Lockerbie, S. D. Keil, P. H. Ruane, M. S. Platz, C. B. Martin, J-L. Ravanat, J. Cadet, and R. P. Goodrich. Riboflavin and uv-light based pathogen reduction: extent and consequence of dna damage at the molecular level. *Photochemistry and Photobiology*, 2004.

[8] E. B Podgorsak. *Radiation physics for medical physicists*. Springer-Verlag, 2016.

[9] J-P. Pouget, S. Frelon, J-L. Ravanat, I. Testard, F. Odin, and J. Cadet. Formation of modified dna bases in cells exposed either to gamma radiation or to high-let particles. *Radiation Research*, 2002.

[10] R. D. Stewart, V. K. Yu, Georgakilas, Alexandros G., C. Koumenis, J. Park, and D. J. Carlson. Effects of radiation quality and oxygen on clustered dna lesions and cell death. *Radiation Research*, 2011.

[11] A. Urushibara, N. Shikazono, P. O'Neill, K. Fujii, S. Wada, and A. Yokoya. Let dependence of the yield of single-, double-strand breaks and base lesions in fully hydrated plasmid dna films by 4he(2+) ion irradiation. *International Journal of Radiation Biology*, 2008.

[12] T. Ushigome, N. Shikazono, K. Fujii, R. Watanabe, M. Suzuki, C. Tsuruoka, H. Tauchi, and A. Yokoya. Yield of single- and double-strand breaks and nucleobase lesions in fully hydrated plasmid dna films irradiated with high-let charged particles. *Radiation research*, 2012.

[13] T. Watanabe, K. Makitsuru, H. Nakazawa, S. Hara, T. Suehiro, A. Yamamoto, T. Hiraide, and T. Ogawa. Separation of double-strand dna fragments by high-performance liquid chromatography using a ceramic hydroxyapatite column. *Analytica Chimica Acta*, 1999.